Journal of the Association for Research in Otolaryngology (2023) 24:305–324
https://doi.org/10.1007/s10162-023-00892-4

JARO

ORIGINAL ARTICLE

Bandpass Shape of Distortion-Product Otoacoustic Emission Ratio Functions Reflects Cochlear Frequency Tuning in Normal-Hearing Mice

James B. Dewey[1] · Christopher A. Shera[1,2]

Received: 19 September 2022 / Accepted: 2 February 2023 / Published online: 18 April 2023
© The Author(s) 2023

Abstract

The frequency selectivity of the mammalian auditory system is critical for discriminating complex sounds like speech. This selectivity derives from the sharp tuning of the cochlea's mechanical response to sound, which is largely attributed to the amplification of cochlear vibrations by outer hair cells (OHCs). Due to its nonlinearity, the amplification process also leads to the generation of distortion products (DPs), some of which propagate out to the ear canal as DP otoacoustic emissions (DPOAEs). However, the insight that these signals provide about the tuned micro- and macro-mechanics underlying their generation remains unclear. Using optical coherence tomography to measure cochlear vibrations in mice, we show that the cochlea's frequency tuning is reflected in the bandpass shape that is observed in DPOAE amplitudes when the ratio of the two evoking stimulus frequencies is varied (here termed DPOAE "ratio functions"). The tuning sharpness of DPOAE ratio functions and cochlear vibrations co-varied with stimulus level, with a similar quantitative agreement in tuning sharpness observed for both apical and mid-cochlear locations. Measurement of intracochlear DPs revealed that the tuning of the DPOAE ratio functions was not caused by mechanisms that shape DPs locally near where they are generated. Instead, simple model simulations indicate that the bandpass shape is due to a more global wave interference phenomenon. It appears that the filtering of DPOAEs by wave interactions over an extended spatial region allows them to provide a window onto the frequency tuning of single cochlear locations.

Keywords Frequency selectivity · Distortion-product otoacoustic emission · Cochlea · Outer hair cell · Optical coherence tomography

Introduction

In mammals, the ability to discriminate and segregate sounds with similar frequency content depends on an active amplification process mediated by the cochlear outer hair cells (OHCs) [1]. While passive gradients in the stiffness of the basilar membrane (BM) underlie the cochlea's fundamental frequency-to-place mapping, such that low-frequency sounds elicit waves on the BM that peak at the cochlear apex, and high-frequency sounds elicit waves that peak toward the base [2], the frequency tuning of each location is dramatically enhanced by the OHCs. OHCs first detect vibrations of the underlying BM via deflection of their mechanotransducing stereociliary bundles and then generate force in response [3, 4]. These forces amplify traveling waves in a frequency-selective manner [1, 5, 6], thus increasing and sharply tuning the mechanical input to the inner hair cells (IHCs), the cochlea's primary afferent receptors communicating with the auditory nerve.

While responsible for the cochlea's remarkable frequency selectivity, the amplification process is also highly nonlinear, resulting in the generation of distortion products (DPs) at frequencies not present in the acoustic stimulus. The nonlinearity is primarily attributed to OHC mechanotransduction, which introduces DPs into the electrical potentials that drive OHC force generation, thus initiating waves at DP frequencies [7]. Some of these waves travel to the stapes and are transmitted to the ear canal where they can

✉ James B. Dewey
jamesdew@usc.edu

Christopher A. Shera
christopher.shera@usc.edu

[1] Caruso Department of Otolaryngology - Head and Neck Surgery, University of Southern California, Los Angeles 90033, CA, USA

[2] Department of Physics and Astronomy, University of Southern California, Los Angeles, CA 90089, USA

be recorded as distortion-product otoacoustic emissions (DPOAEs) [8]. Typically elicited by two tones at frequencies f_1 and f_2 ($f_2 > f_1$) and measured at related frequencies such as $2f_1 - f_2$, DPOAEs provide a noninvasive window onto cochlear mechanics. However, due to complexities in how these signals are generated and propagate, it remains uncertain whether DPOAEs provide any precise information about the nonlinear, frequency-selective processes that generate them. To address this, the present report examines a phenomenon observed in DPOAE recordings that has long been suggested to relate to cochlear frequency tuning — namely, the bandpass shape observed in $2f_1 - f_2$ DPOAE amplitudes as the ratio of the two stimulus frequencies is varied from large to small [9–12].

Originally attributed to a resonance of the tectorial membrane (TM) overlying the OHCs [13–15], the bandpass shape in DPOAE amplitude vs. f_2/f_1 ratio functions (referred to here as "ratio functions") has also been proposed to be due to suppression [16], the form of the underlying nonlinearity [17], and interference between DP waves generated at different locations [18–21]. These mechanisms all theoretically depend on or involve the sharpness of cochlear tuning, suggesting a relationship between the tuning of cochlear vibrations and DPOAE ratio functions. Though the tuning of DPOAE ratio functions is only modestly correlated with psychophysical measures of tuning in humans [22, 23], the latter are likely influenced by central properties, and it is unclear how they relate to cochlear tuning, specifically. Modeling of human DPOAE generation suggests that cochlear tuning can be predicted from DPOAE ratio functions [24]; however, the necessary assumptions regarding human cochlear mechanics remain speculative.

Here, we explicitly tested this relationship in mice by using optical coherence tomography to measure cochlear vibrations, and then comparing the tuning of these responses with the tuning of DPOAE ratio functions measured in the same ears. Additionally, we used intracochlear DP measurements and a simple model to test whether DPOAE ratio functions are tuned by local mechanisms that shape DPs where they are generated, or by a more global mechanism such as wave interference.

Methods

Mouse Preparation

DPOAEs and cochlear vibrations were measured from adult (4–7 week old) wild-type CBA/CaJ mice of either sex ($n = 29$, 15 female). Mice were bred and housed on-site at the University of Southern California, and all procedures were approved by the local Institutional Animal Care and Use Committee.

Mice were anesthetized (80 mg/kg ketamine, 10 mg/kg xylazine) and placed on a heating pad to maintain body temperature at ~ 38 °C, with additional anesthesia administered to ensure areflexia for the duration of the experiment. After fixing the skull to a head-holder with dental cement, the left bulla was accessed using a ventrolateral surgical approach. The bone below the tympanic annulus was then removed to widely expose the middle ear space and otic capsule. Resection of the pinna and ear canal facilitated placement of the tip of an acoustic probe (ER10-X; Etymotic Research, Elk Grove, IL) within a few mm of the tympanic membrane, with the probe tip coupled to the residual ear canal via plastic tubing. The tubing was glued in place to create a stable and closed acoustic field. After all desired measurements were completed, mice were euthanized by anesthetic overdose. Measurements were often repeated postmortem to ensure the absence of any artifactual distortion in the in vivo responses. Postmortem vibrations of the ossicular chain were also measured in a subset of mice in order to quantify delays associated with middle-ear transmission.

Optical Coherence Tomography

Cochlear vibrations were measured in response to single- and two-tone stimuli using a custom-built optical coherence tomography (OCT) system that has previously been described in detail [5, 25–27]. Briefly, the system employs an akinetic swept laser with a 1310-nm center wavelength, 95-nm bandwidth, and 100-kHz sweep rate (Insight Photonic Solutions, Inc., Lafayette, CO). Light reflected from the sample was combined with the light from a reference mirror in order to generate interferograms, which were digitized at 12-bit resolution and 400 MS/s (AlazarTech ATS9373 card; Alazar Technologies Inc., Pointe-Claire, QC, Canada). Custom software (written in Python, CUDA, and C++) was used in conjunction with National Instruments hardware (Austin, TX) to generate stimulus waveforms, control the mirror used to scan the laser across the sample, and process the interferometric signals. The axial and lateral imaging resolutions of the system were ~ 12.5 and ~ 9.8 μm, respectively, and the displacement measurement noise floor was typically ~ 0.01 to 0.1 nm depending on the amount of time-domain averaging used and the reflectivity of the measurement location.

After opening the bulla, the laser was scanned across the cochlear bone to obtain cross-sectional images (Fig. 1A). The mouse's head was adjusted so that the BM in the apical turn was oriented roughly orthogonal to path of the laser, with the angle between the BM surface and the beam path being at least 60°. Only displacements in line with the beam path were measured, such that the recordings were likely dominated by the transverse motion of the structures. However, radial and/or longitudinal motions may also have contributed to the measured signal.

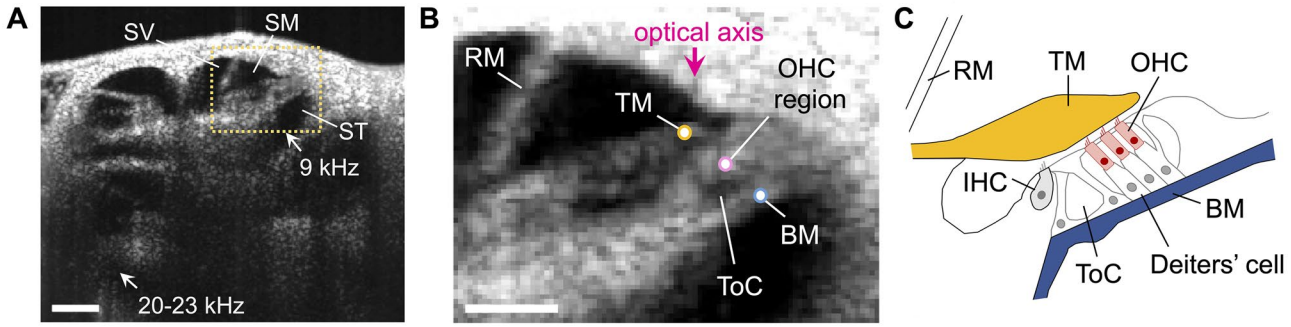

Fig. 1 OCT imaging of the mouse cochlea. **A** Cross-sectional OCT image of the live mouse cochlea. The three fluid-filled scalae are labeled (SV = scala vestibuli, SM = scala media, ST = scala tympani). Highlighted is the apical region tuned to 9 kHz, where vibrations were typically measured. Also indicated is the middle-turn region tuned to 20–23 kHz, where limited additional measurements were made. Scale bar = 200 µm. **B** Magnified cross-section of the 9 kHz region highlighted in (**A**). Indicated are the approximate points on the BM, OHC region, and TM from which vibrations were measured. Vibration measurements captured motions in line with the optical axis. Also indicated are the tunnel of Corti (ToC) and Reissner's membrane (RM). Scale bar = 100 µm. **C** Schematic showing the relevant anatomy

We primarily measured vibrations from an apical cochlear region tuned to a characteristic frequency (CF) of 9 kHz, where displacements were measured from the BM, OHC region, and TM (Fig. 1B, C). Positions of various measurement points were inferred from the known anatomy [28]. Measurements were obtained from the BM near its midpoint, where vibrations are maximal [25], while OHC region measurements were obtained near the junction between the OHCs and their underlying supporting cells (the Deiters' cells), which connect the OHCs to the BM. TM measurements were obtained from a point above the apical ends of the OHCs, roughly halfway between the TM's lower and upper surfaces. Since it was not always possible to clearly visualize the TM, measurements may have been closer to the lower or upper surface in certain preparations. To ensure a high signal-to-noise ratio, measurements were always obtained from highly reflective points (i.e., bright pixels in the cross-sectional images).

In six mice, we obtained vibrations from mid-cochlear regions with CFs of 20–23 kHz, which we will refer to as "middle-turn" locations. Since the light reflected from the middle turn was weak, it was difficult to discern any individual structures or features, with the BM and organ of Corti appearing as a grainy, partially obscured mass. Nevertheless, interpretable vibration data were obtained from points at the bottom or top of the partition, and the responses exhibited nonlinear characteristics similar to those observed in the apical turn.

Single- and Two-Tone Stimulus Paradigms

Responses to single tones were used to quantify cochlear frequency tuning, while two-tone stimuli were used to elicit intracochlear DPs and DPOAEs. All stimuli were 102 ms in duration, with 1 ms ramps applied to the beginning and end of the stimulus waveform, and were presented once every ~ 110 ms. Stimuli were calibrated using the pressure measured by the probe microphone, after compensating for its frequency-dependent transfer function.

In apical measurements, single-tone responses were obtained at frequencies from 1 to 15 kHz in 0.5 kHz steps. We first obtained BM responses for tones presented at 30 dB sound pressure level (SPL) so as to determine the CF of the measurement site, which was defined as the frequency eliciting the maximum response. Displacements were then obtained from the BM, OHC region, and TM with stimuli presented from 10 to 90 dB SPL in 10 dB steps. In later experiments, additional measurements were obtained from 30 to 75 dB SPL in 5 dB steps, so as to cover the same range of same stimulus levels over which DPOAEs were also typically measured. In middle-turn measurements, single-tone responses were obtained from 1 to 30 kHz in 0.5 or 1 kHz steps with stimulus levels varied from 30 to 90 dB SPL in 10 dB steps. Single-tone responses were averaged over 1–16 stimulus repetitions, with 8 stimulus repetitions being used in the majority of measurements.

Two-tone responses were obtained with the higher-frequency f_2 tone fixed near the CF of the measurement site and the f_1 tone varied to achieve f_2/f_1 ratios of ~ 1.02–1.87 in 0.025 steps. In one paradigm, the levels of the f_1 and f_2 tones were the same and varied from 30 to 70 dB SPL in 10 dB steps or 30 to 75 dB SPL in 5 dB steps. In a second paradigm used to examine the influence of suppression, the level of the f_2 tone was fixed at 60 dB SPL and the f_1 tone was varied from 45 to 75 dB SPL in 5 dB steps. Responses were averaged over 8–32 stimulus repetitions.

For all measurements, a fast Fourier transform was applied to the steady-state portion of the average response in order to extract the magnitude and phase at the stimulus and DP frequencies. Stimulus frequencies were rounded to the nearest 10 Hz so that the steady-state response included an integer number of stimulus cycles. The noise floor for each response component was taken as the mean + 3 standard

deviations (SDs) of the magnitudes in nearby frequency bins (± 220–320 Hz for responses at the stimulus frequencies, and ± 20–120 Hz for DPs). Response phases were referenced to the phase of the stimulus pressure measured in the ear canal. For DPs and DPOAEs at $2f_1 - f_2$, this involved subtracting $2\varphi_{1ec} - \varphi_{2ec}$ from the response phase, where φ_{1ec} and φ_{2ec} were the phases of the f_1 and f_2 stimuli in the ear canal, respectively.

Initially, vibratory and ear-canal responses to two-tone stimuli were only obtained simultaneously. However, we found that keeping the number of stimulus repetitions to ~ 8–16 was necessary to cover all stimulus frequencies and levels without drift in the reflectivity of the measurement point over time. While avoiding such drift was required to obtain clean vibratory responses, using a low number of stimulus repetitions also resulted in a higher noise floor in the DPOAE measurements. Acoustic noise from the OCT system's scanning mirror and electrical noise from National Instruments hardware were also sometimes problematic. Thus, in later experiments, we obtained DPOAE measurements using an RME Babyface audio interface (Audio AG, Haimhausen, Germany) and software (ARLas, provided by Dr. Shawn Goodman, https://github.com/myKungFu/ARLas) written in MATLAB (MathWorks, Natick, MA), using a 192-kHz sampling rate. Responses were averaged over 32 stimulus repetitions but were otherwise obtained using identical parameters, and the resulting DPOAEs were consistent with those obtained during the two-tone OCT measurements. The reduced noise floors in the RME audio interface recordings facilitated calculation of DPOAE tuning sharpness at lower stimulus levels.

For middle-turn measurements, the higher displacement noise floors precluded characterization of the intracochlear DPs, such that two-tone responses were only obtained from the ear canal. For these measurements, we first used OCT to measure single-tone vibratory responses, and then used the RME interface to obtain DPOAE ratio functions with f_2 set near the CF of the measurement site. As the vibratory measurements from the middle turn were somewhat challenging, multiple attempts to record clean responses were made both before and after the DPOAE measurements, which sometimes involved repositioning of the mouse to improve the OCT image. Thus, the CF of the recording site which ultimately yielded the cleanest data was not always identical to the f_2 frequency used in the DPOAE measurements, differing by ~ 1 kHz (~ 0.1 octave) in three of the six mice. Since cochlear tuning is expected to vary only slowly with location [29], such differences likely have little impact on the results.

As we did not wish to artificially minimize variability in cochlear sensitivity and tuning across mice, we did not first obtain auditory brainstem responses to screen for normal hearing function. Nevertheless, all preparations were considered to have essentially normal mechanical sensitivity, with displacement responses to low-level tones varying by less than 12 dB for a given measurement location. For apical measurements, BM responses to CF tones presented at 30 dB SPL ranged in magnitude from 0.9 to 2.6 nm, falling at most 2.6 dB below to 6.4 dB above the average response (1.24 nm). In middle-turn measurements from both the bottom and top of the organ of Corti, CF responses to 30 dB SPL tones ranged in magnitude from 0.3 to 1.12 nm, falling at most 4.8 dB below to 6.7 dB above the average response (0.52 nm). When obtained using the optimal f_2/f_1 ratio for a given f_2 frequency, DPOAE amplitudes always exceeded -5 dB SPL for equal-level stimuli presented at 40 dB SPL or higher. For a given f_2 frequency and stimulus level, DPOAE amplitudes all fell within a 10-dB range.

Quantifying Tuning Sharpness

We quantified the tuning of vibratory responses to single tones by dividing the frequency eliciting the peak displacement response by the bandwidth 10 dB below the peak, yielding the Q_{10dB}. For DPOAE measurements, we calculated Q_{10dB} in the same manner, with DPOAE amplitudes plotted and analyzed with respect to the DP frequency. To verify that the results held across different metrics of tuning, we also calculated the equivalent rectangular bandwidth (ERB) of the responses by normalizing the amplitudes (in linear units) to their maximum, squaring the normalized amplitudes to be proportional to power, and then computing the area under the curve. Dividing the response's peak frequency by the ERB yielded the Q_{ERB}. When multiple measurements of either DPOAE ratio functions or vibratory responses were obtained in a single preparation, Q_{10dB} or Q_{ERB} was calculated for each individual measurement and then averaged across all measurements to obtain the final value ($n = 1$–5 across preparations).

Unlike in recent human studies [23, 24], we quantified the tuning of DPOAE ratio functions without first attempting to the reduce the influence of so-called "reflection" components in the responses, which arise from backscattering of DP waves as they propagate apically to the place tuned to the DP frequency [30]. These reflections can interfere with components originating from near the place tuned to f_2 to produce peaks and valleys in the measured responses, potentially complicating tuning estimates. While signal-processing techniques can help to separate and attenuate the reflection component based on its distinct phase-vs.-frequency behavior [24], we did not apply these techniques in the present study, as the delays of emissions arising from reflection are very short (< 1 ms) in mice [31], making it difficult to cleanly separate the reflection component. Furthermore, such component separation appeared unnecessary, as DPOAE amplitudes typically varied smoothly with frequency, indicating that any reflection components were negligible. This is

consistent with previous studies in other rodents, which have also found that reflection components are small [32]. Though ratio functions obtained with high f_2 frequencies sometimes exhibited stronger amplitude fluctuations, these typically occurred at DP frequencies distant from the dominant peak of the functions and so were unlikely to influence tuning estimates. Thus, for simplicity, we quantified tuning using the raw ratio functions.

Modeling Wave Interference

We implemented a simple model in MATLAB to determine the influence of wave interference on DPOAEs. Using the frequency-to-place map of the mouse cochlea [33], we estimated the displacements evoked by a given pair of f_1 and f_2 tones as a function of cochlear distance (0–5.13 mm from the base, in 0.01 mm steps) by extrapolating from average BM frequency responses ($n = 22$) at the 9-kHz location. To ensure that the BM phases only reflected delays associated with traveling-wave propagation, the average phases of postmortem middle-ear vibrations ($n = 22$) were first subtracted from the BM responses. Averaged across frequency, the mean middle-ear delay was ~ 36 µs.

To generate DPs at each cochlear location, displacements at f_1 and f_2 were given as inputs to a first-order Boltzmann function, which we used to approximate the nonlinear relationship between OHC stereociliary bundle deflection and the resulting mechanotransduction current. The function is given by:

$$y(x) = 1/(1 + e^{a_1(x_1 - x)}), \quad (1)$$

where y is the current, x is the instantaneous bundle position, a_1 sets the slope of the function (here, 0.28 nm^{-1}), and x_1 is the position of maximum slope (here, 2.6 nm). Since the changes in membrane potential that drive OHC force generation are low-pass filtered by the membrane's electrical properties [34–36], the Boltzmann's output was low-pass filtered using a corner frequency 2.36 octaves below the local CF. The Boltzmann and low-pass filter parameters were derived in a previous analysis of vibratory nonlinearities in the 9-kHz location [25]. While this analysis focused on fitting the parameters to replicate the level-dependent growth of harmonic and tonic distortions in single-tone responses of the OHC region, these same parameters have recently been shown to also approximate the growth of the $2f_1 - f_2$ DP [37].

The magnitude and phase of the low-pass filtered output at $2f_1 - f_2$ were taken to be those of the locally generated DP. To estimate the DP arriving at the stapes, we assumed that each locally generated DP produced a reverse-propagating wave coupled to BM motion. Thus, DP magnitudes at each location were scaled by the BM displacement that would be driven by a low-level (40 dB SPL) tone at the DP frequency. Likewise, the phase of each DP was shifted to account for the phase delay due to reverse propagation, which we assumed to be the local phase of a forward-traveling BM wave at the DP frequency. These adjustments are admittedly crude and ignore the physics of how OHC generated forces couple to BM motion and produce the pressure waves that lead to DPOAEs (e.g., [38]). However, as mentioned below, exploration of the model's output indicates that such details are unlikely to fundamentally change the predicted effects of wave interference. To estimate the total resulting DPOAE, we vectorially summed the BM-displacement-weighted DPs arriving at the stapes from all locations.

Though the assumption of reverse DP propagation primarily through "slow" traveling waves is supported by abundant experimental data and modeling efforts [39–44], an alternative hypothesis is that DPs propagate to the stapes through "fast" compression waves in the cochlear fluid [45, 46]. DPs propagating in reverse through fast waves would experience little delay, potentially leading to differences in how they interfere. In the end, however, assuming reverse DP propagation through either fast or slow waves did not qualitatively affect the model's output, and, thus, did not alter our primary conclusions.

We also tested whether similar results were obtained when using average middle-turn vibrations ($n = 6$) to estimate DPOAE ratio functions for an f_2 of 20 kHz. The phases of middle-turn vibratory responses below or above 15 kHz were corrected using average middle-ear measurements obtained in 22 or 10 mice, respectively. Responses from different locations were then expressed in octaves relative to the CF and interpolated prior to averaging. Due to the lower signal-to-noise ratio and phase irregularities at frequencies above the CF, it was unfortunately not possible to estimate traveling wave responses at locations greater than 0.32 mm apical to each response's peak. This effectively limited the DP generation in the model to locations no more than 0.32 mm apical to the f_2 place. However, we do not anticipate that this significantly affected the estimated ratio functions, as the magnitudes and phases of the modeled DPs indicated that the dominant DPOAE sources were basal to this location. Moreover, imposing a similar limitation on the model using the apical data had little effect on the estimated ratio functions.

Experimental Design and Statistical Analyses

Statistical analyses were performed using MATLAB and SPSS (IBM Corp, Armonk, NY). Vibratory and DPOAE Q_{10dB} values were compared with repeated-measures ANOVA, with stimulus level and measurement location (i.e., BM, OHC region, TM, and ear canal) as within-subjects factors. Vibratory Q_{10dB} values for apical and middle-turn CF regions were compared using a two-way mixed ANOVA, with CF (apical vs. middle turn) as a between-subjects factor and stimulus level as a within-subjects

factor. Results of repeated-measures ANOVA were adjusted for violations of sphericity using Greenhouse–Geisser corrections when applicable, and pairwise comparisons were performed using Bonferroni corrections. Pearson's correlations were applied to further describe the strength of the relationship between vibratory and DPOAE Q_{10dB} values. Paired or unpaired *t* tests were used to compare characteristics of vibratory and DPOAE responses. For all *F* and *t* statistics, degrees of freedom are provided in parentheses. Unless noted otherwise, reported values are the mean ± 1 standard error (SE) and only data with magnitudes exceeding the measurement noise floor are analyzed or plotted. All reported displacement magnitudes are the root-mean-square values.

Results

The Tuning Sharpness of Cochlear Vibrations and DPOAE Ratio Functions is Highly Similar

We used OCT to measure sound-evoked vibrations from within the mouse cochlea so that the tuning of the vibratory responses could be compared with the tuning of DPOAE ratio functions from the same ear. Representative displacement responses to single tones are shown for an apical cochlear region tuned to a CF of 9 kHz in Fig. 2A–C. At low stimulus levels, displacements of the BM, OHC region, and TM were all sharply tuned to the CF, while at higher stimulus levels, the responses became more broadly tuned and peaked at slightly lower frequencies. This broadening of tuning with increasing level is due to the inherent nonlinearity and frequency selectivity in the OHC-mediated amplification process, which causes responses near the CF to grow compressively and saturate with increasing stimulus level, and responses at lower frequencies to grow more linearly. Also shown are the displacement phases, which increasingly lag with frequency, reflecting the delays associated with traveling wave propagation.

DPOAE ratio functions obtained from the same ear were also sharply tuned, exhibiting a pronounced bandpass shape (Fig. 2D). With f_2 fixed at 9 kHz and f_1 varied, DPOAE amplitudes reliably peaked at an f_2/f_1 ratio near ~ 1.3 (i.e., when $f_1 \approx$ 7 kHz and $2f_1 - f_2 \approx 5$ kHz) and rapidly decreased at smaller or larger ratios. While the f_2/f_1 ratio producing the largest DPOAE varied little across stimulus level, DPOAE ratio functions became more broadly tuned as the stimulus level was increased. DPOAE phases also accumulated multiple cycles of lag with increasing DP frequency (i.e., decreasing f_2/f_1 ratio), though the total phase lag was ~ 2–2.5 times that observed for the vibratory responses to single tones over this same frequency range. As the interpretation of DPOAE phases measured using the fixed-f_2, swept-f_1 stimulus paradigm remains uncertain [47], we focus our analyses primarily on DPOAE amplitudes.

To explicitly compare the tuning sharpness of cochlear vibrations and DPOAE ratio functions, we divided the frequency of

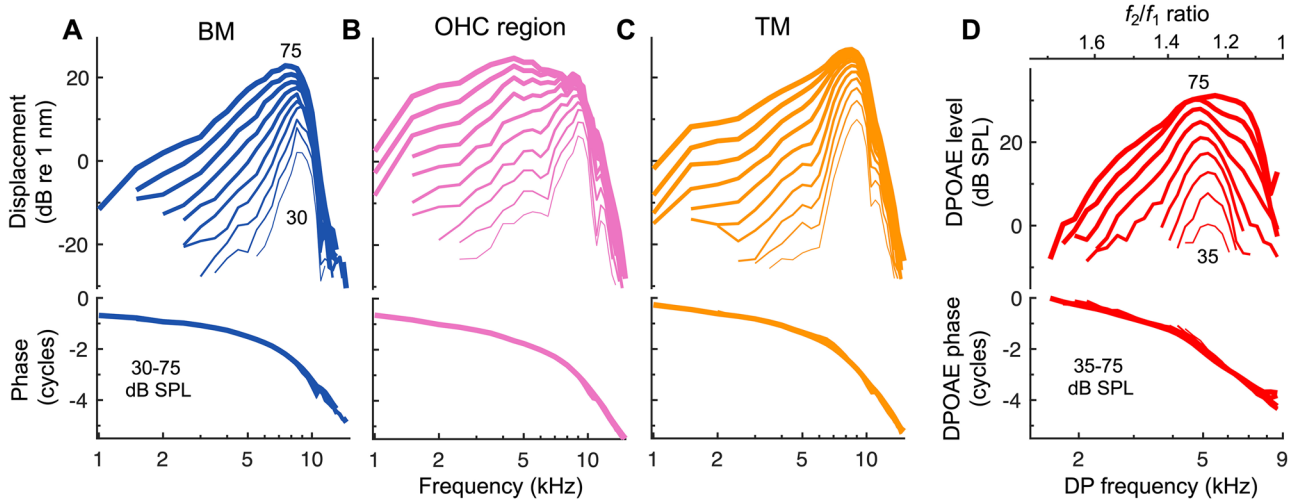

Fig. 2 The tuning sharpness of cochlear vibrations and DPOAE ratio functions is level dependent. **A**–**C** Displacement amplitudes (top) and phases (bottom) of the BM (**A**), OHC region (**B**), and TM (**C**) in response to single tones for an individual mouse. Stimuli were swept in frequency (1–15 kHz in 0.5 kHz steps) and level (30–75 dB SPL in 5 dB steps). Responses for higher levels are indicated by increasing line thickness, with 30 and 75 dB SPL responses indicated numerically in (**A**). Phases were referenced to the phase of the stimulus pressure in the ear canal. All responses exhibit compressive, nonlinear growth near the CF and broader tuning with increasing stimulus level. **D** Amplitude and phase of the $2f_1 - f_2$ DPOAE measured in the ear canal of the same mouse with f_2 fixed at 9 kHz and f_1 varied. The f_2 and f_1 tones were presented at the same level, from 30 to 75 dB SPL in 5 dB steps, though DPOAEs were typically only measurable above the noise floor for stimulus levels of 35 dB SPL or higher. Phases were referenced to $2\varphi_{1ec} - \varphi_{2ec}$, where φ_{1ec} and φ_{2ec} were the phases of the f_1 and f_2 stimuli in the ear canal. In all panels, only responses with magnitudes meeting the signal-to-noise criterion are shown (see Methods)

maximum response for a given stimulus level by the bandwidth 10 dB below to calculate the Q_{10dB} value (Fig. 3A). Q_{10dB} values for DPOAE ratio functions were remarkably similar to those of BM and TM vibrations across a wide range of stimulus levels, decreasing by a factor of ~2 as stimulus levels increased from 40 to 75 dB SPL (Fig. 3B). Q_{10dB} values for OHC region vibrations were comparable at stimulus levels below 40 dB SPL, though they tended to decrease more rapidly with increasing stimulus level. The broader tuning of the OHC region is due to a low-pass characteristic that may reflect membrane filtering of the receptor potential, and thus the OHC's motile response [25, 48].

While the correspondence between Q_{10dB} values for DPOAEs and vibratory responses in individual mice was not always as close as that shown in Fig. 3B, we found a strong relationship in the average data (Fig. 3C). Average Q_{10dB} values for DPOAE ratio functions were nearly indistinguishable from those of the BM for all stimulus levels except 50 dB SPL, where they were closer to those of the TM. When considering only data obtained with stimulus levels of 50–70 dB SPL, for which Q_{10dB} values could be calculated for all measurements in 13 mice, a repeated-measures ANOVA revealed significant effects of both measurement location/type ($F(1.75,21.04) = 67.01$, $P < 0.001$) and stimulus level ($F(1.37,16.45) = 674.49$, $P < 0.001$), and no significant interaction between measurement location/type and stimulus level ($F(2.46,29.51) = 1.86$, $P = 0.17$). Pairwise comparisons between measurement locations/types confirmed that OHC region responses were significantly more broadly tuned than the other types of responses ($P < 0.001$), and BM Q_{10dB} values were slightly but significantly lower than TM Q_{10dB} ($P < 0.001$). However, Q_{10dB} values for DPOAE ratio functions were not significantly different from those of either the BM ($P = 0.18$) or TM responses ($P = 0.34$).

When including data at all levels (40–70 dB SPL in 10 dB steps), DPOAE Q_{10dB} values were positively and significantly correlated with BM Q_{10dB} ($R^2 = 0.83$, $P < 0.001$) and TM Q_{10dB} ($R^2 = 0.81$, $P < 0.001$). However, DPOAE and vibratory Q_{10dB} values were not significantly correlated when considering the data for any one stimulus level. A weak or absent correlation is not unexpected given that all mice had normal cochlear sensitivity, such that the variance in vibratory or DPOAE responses should be low and perhaps largely attributed to measurement noise. However, we note that the morphology of the DPOAE responses was also somewhat more variable across mice when compared to the vibratory responses, with diverse and nonmonotonic (albeit small) shifts in the optimal f_2/f_1 ratio and DPOAE frequency with changes in stimulus level, which impacted the DPOAE Q_{10dB} values. This variable morphology was likely of physiological or acoustic origin, as it was observed even when DPOAE magnitudes were significantly above the measurement noise floor. On average, the variance in DPOAE Q_{10dB} values for a given stimulus level was twice that observed in the vibratory responses. Nevertheless, the absolute percentage difference between DPOAE and BM or TM Q_{10dB} values obtained in individual ears was at most 32.2%, and only 10.1% on average.

To verify that the similarity in tuning sharpness did not depend on the specific metric used, we also calculated the equivalent rectangular bandwidth (ERB) of each curve. Dividing the frequency of maximum response by the ERB yielded the Q_{ERB}, which revealed essentially the same close

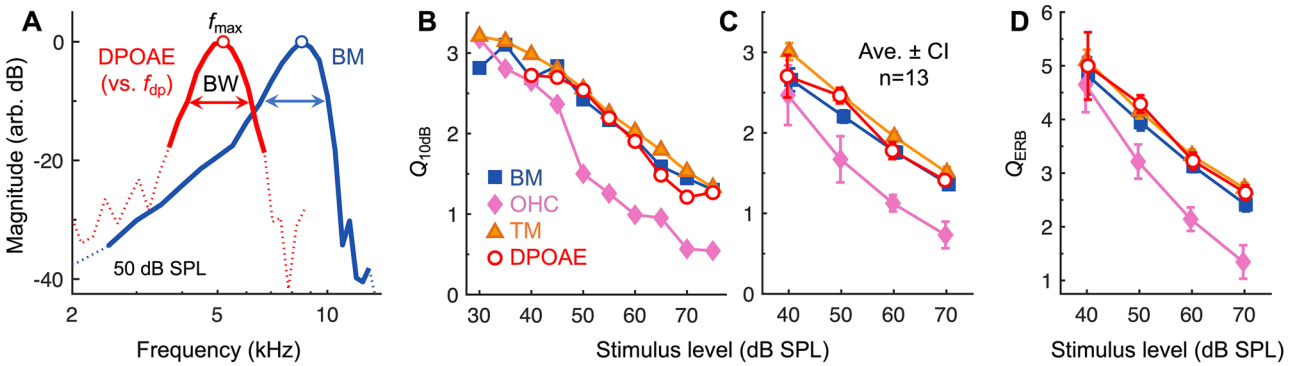

Fig. 3 The tuning sharpness of cochlear vibrations and DPOAE ratio functions is highly similar. **A** Single-tone BM responses and DPOAE ratio function amplitudes for stimuli presented at 50 dB SPL. Data are from Fig. 2A, D with DPOAEs plotted vs the DP frequency (f_{dp}) and both responses normalized to their maximum. Tuning sharpness was quantified by dividing the frequency of the response peak (f_{max}) by the bandwidth (BW) 10 dB down, yielding the Q_{10dB}. Data not meeting the signal-to-noise criterion are shown with dotted lines, illustrating that this criterion was strict enough to yield Q_{10dB} values that weren't strongly influenced by noise. **B** Q_{10dB} vs. stimulus level for the cochlear vibrations and DPOAE ratio functions shown in Fig. 2. The tuning of the DPOAE ratio functions was similar to BM and TM tuning over a wide range of stimulus levels. OHC region tuning was often broader, particularly at high stimulus levels. **C** Average Q_{10dB} (±95% CI) for cochlear vibrations and DPOAE ratio functions obtained with 40–70 dB SPL stimuli. Averages are from 13 mice in which both the CF and f_2 were 9 kHz. For 40 dB SPL stimuli, DPOAE tuning could only be quantified in seven mice. **D** Average tuning sharpness (±95% CI) for cochlear vibrations and DPOAE ratio functions expressed in Q_{ERB}, demonstrating that the correspondence holds for different tuning metrics

relationship between the tuning of DPOAE ratio functions and the tuning of BM and TM vibrations (Fig. 3D). Average DPOAE Q_{ERB} tended to be more similar to TM Q_{ERB}, rather than BM Q_{ERB}, although any differences were small. When including data for all stimulus levels, absolute percentage differences between DPOAE and BM or TM Q_{ERB} values were 9% on average.

Tuning of DPOAE Ratio Functions and Cochlear Vibrations is Similar at Higher CFs and f_2 Frequencies

To test whether the agreement in tuning sharpness extends to other CF regions and f_2 frequencies, we measured vibrations from more basal, middle-turn locations with CFs of 20–23 kHz (average CF = 21.3 kHz) (Fig. 4). Due to the low reflectivity of the structures in the middle turn, the image quality and vibratory signal-to-noise ratio were poorer compared to the apical measurements. However, it was still possible to measure sensitive and sharply tuned vibrations from a region that presumably comprised the BM and organ of Corti (Fig. 4A, B). Vibration measurements were obtained from reflective points at approximately the bottom ($n = 4$) or top ($n = 2$) of this region, likely near the BM or reticular lamina/TM, respectively.

To provide assurance of this, BM responses from the 9 and 21 kHz regions in the same mouse are compared in Fig. 4C, with displacements normalized to the evoking sound pressure to highlight the nonlinearity in the responses. While displacements from the middle turn were smaller than those in the apex, they exhibited a similar amount of nonlinear, compressive growth near the CF. This is demonstrated by the decrease in the normalized response magnitude with increasing stimulus level. For quantitative purposes, we took the difference between the normalized CF responses at 30 and 90 dB SPL as the amount of nonlinear "gain". Middle-turn gains were 40.5 ± 2.6 dB ($n = 6$), which were comparable to apical BM gains (41.1 ± 0.7 dB, $n = 13$; not significantly different by t-test, $t(17) = 0.28$, $P = 0.78$). Gains for the two middle-turn measurements made near the top of the organ of Corti (42.6 and 50.3 dB) were among the three highest observed. This is consistent with the greater gain in TM vs. BM responses found in the apex (TM gain = 44.4 ± 0.5 dB; statistically higher than BM gain by paired t-test, $t(12) = 7.87$, $P < 0.001$). Middle-turn displacements also became more broadly tuned and peaked at slightly lower frequencies with increasing stimulus level, though they were always more sharply tuned than the apical responses. Average vibratory Q_{10dB} values were ~ 1.5–1.8 times greater in the 20–23 kHz region than in the 9 kHz region, with greater differences at lower stimulus levels. A two-way mixed ANOVA revealed a statistically significant main effect of measurement location (apical vs. middle turn) on Q_{10dB} ($F(1,17) = 321.28$, $P < 0.001$) and an interaction between stimulus level and measurement location ($F(1.74,29.64) = 43.59$, $P < 0.001$).

Fig. 4 Correspondence between tuning sharpness of cochlear vibrations and DPOAE ratio functions is observed for higher-frequency regions. **A** OCT image of a middle-turn region tuned to 21 kHz. The approximate location of this region within the cochlea is indicated in Fig. 1A. RM is discernible, though the organ of Corti (OoC) is poorly resolved. Measurements were attempted from either the bottom or top of the BM-OoC complex, which is roughly outlined by dotted lines. Scale bar = 100 µm. **B** Displacement responses from the bottom of the BM-OoC complex, presumably near the BM, in an individual mouse. Responses are shown for single tones presented from 30 to 90 dB SPL in 10 dB steps. Responses at the lowest and highest stimulus levels are numerically indicated. Dotted portion of the 60 dB SPL response curve indicates frequencies where data did not meet the signal-to-noise criterion. **C** BM displacements from (**B**) compared with those obtained from the 9 kHz region in the same mouse. Displacements were normalized to the evoking stimulus pressure to highlight the similar degree of nonlinearity near the CF for both apical and middle-turn measurements. Middle-turn displacement phases are consistent with traveling wave propagation to a site closer to the stapes. **D** DPOAE ratio functions from the same mouse with f_2 fixed at the CF (21 kHz) and f_1 varied. Stimuli were varied from 40 to 75 dB SPL in 5 dB steps with the f_1 and f_2 tones presented at the same level. **E** Middle-turn BM responses and DPOAE ratio function amplitudes for stimuli presented at 50 dB SPL. Data are from (**B**) to (**D**) with DPOAEs plotted vs. the DP frequency (f_{dp}) and both responses normalized to their maximum (circles). Data not meeting the signal-to-noise criterion are indicated by dotted lines. **F** Q_{10dB} vs. stimulus level for the middle-turn BM displacements and DPOAE ratio functions shown in (**B**) and (**D**), demonstrating quantitatively similar tuning across stimulus level. **G** Average vibratory and DPOAE Q_{10dB} for six mice in which middle-turn measurements were obtained (CF and f_2 = 20–23 kHz). For 40 dB SPL stimuli, the average and 95% CI are not shown for the DPOAE Q_{10dB}, which could only be quantified in two mice (individual data shown with open symbols)

DPOAE ratio functions obtained with f_2 fixed near the CF of the middle-turn measurement site also resembled those obtained with an f_2 of 9 kHz and exhibited a bandpass shape (Fig. 4D; $f_2 = 21$ kHz). However, they peaked at smaller f_2/f_1 ratios, with an average optimal ratio of 1.14 ± 0.006 ($n = 6$, with optimal ratios first averaged across stimulus level for each mouse). Optimal f_2/f_1 ratios were significantly smaller than those observed for an f_2 of 9 kHz (1.29 ± 0.003, $n = 13$; t-test: $t(17) = 24.03$, $P < 0.001$). Ratio functions for f_2 frequencies of 20–23 kHz or 9 kHz therefore peaked when the DPOAE frequency was ~ 0.4 or ~ 0.9 octaves below f_2, respectively. DPOAE ratio functions obtained with high f_2 frequencies also often contained multiple smaller peaks, as reported previously for measurements in gerbil and guinea pig [15, 49, 50]. Notwithstanding this additional complexity, Q_{10dB} values could be computed from these measurements that were quantitatively similar to those of the middle-turn displacements (Fig. 4E–G).

For Q_{10dB} values derived from middle-turn measurements obtained with stimulus levels of 50–70 dB SPL, a repeated-measures ANOVA (with stimulus level and measurement type

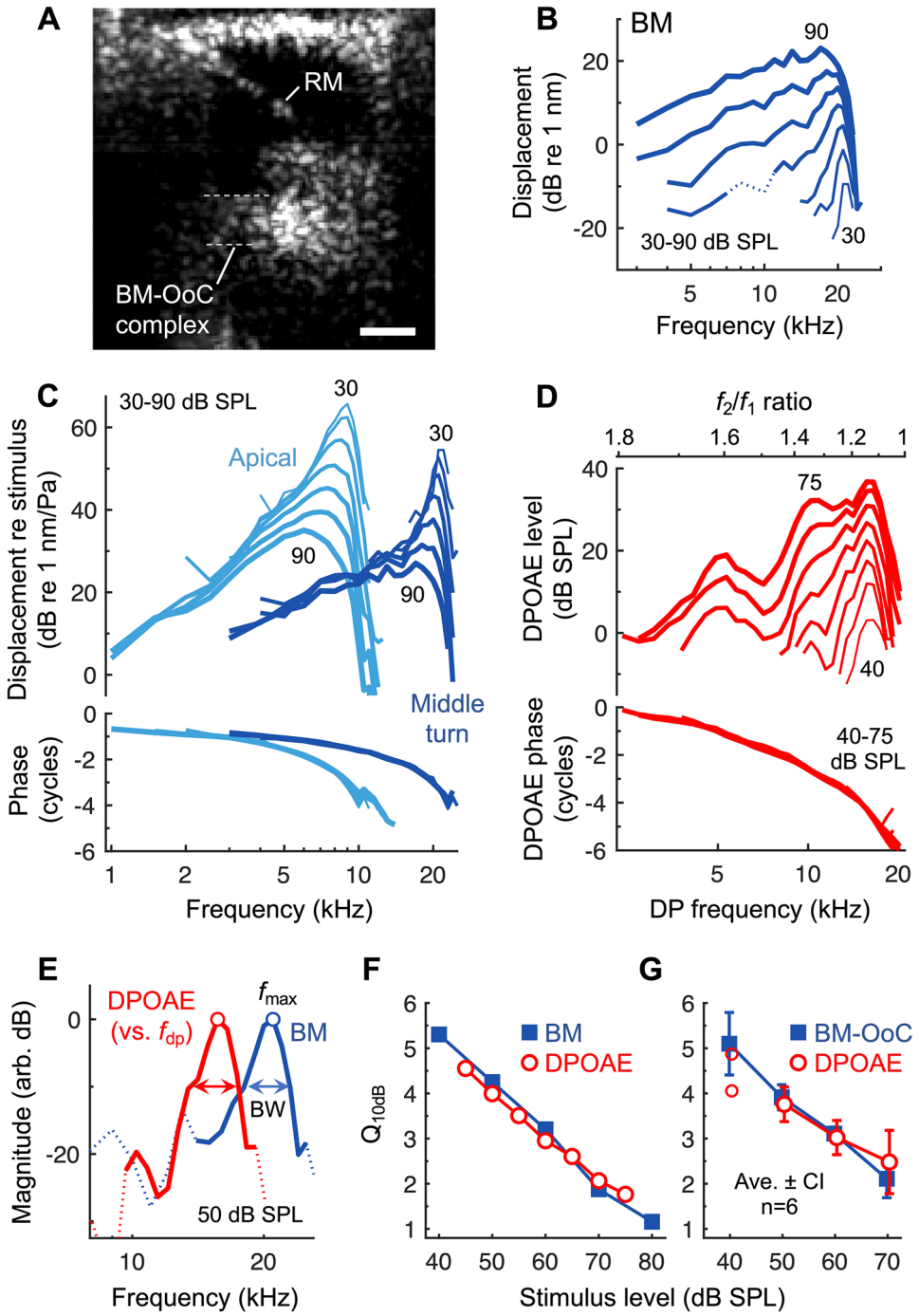

as within-subjects factors) revealed no significant main effect of measurement type ($F(1,5)=0.11$, $P=0.75$), a significant main effect of stimulus level ($F(2,10)=50.35$, $P<0.001$), and a marginally significant interaction between stimulus level and measurement type ($F(2,10)=4.88$, $P=0.03$). When also including data collected at 40 dB SPL, for which it was only possible to quantify DPOAE Q_{10dB} in two mice, absolute percentage differences between DPOAE and vibratory Q_{10dB} values in individual ears were at most 44% and 13.6% on average. Collapsed across stimulus level, DPOAE Q_{10dB} values were positively and significantly correlated with vibratory Q_{10dB} values ($R^2=0.75$, $P<0.001$), though correlations were not significant for any given stimulus level. Thus, we observed a quantitative association between DPOAE and vibratory Q_{10dB} for high CFs and f_2 frequencies similar to that found when the CF and f_2 were 9 kHz.

Tuning of DPOAE Ratio Functions is Not Caused by Filtering at the Site of DP Generation

To determine whether the tuning of DPOAE ratio functions is due to a mechanism that shapes DPs near where they are generated, we next compared DPOAEs to DPs measured in the vibrations of the BM, OHC region, and TM at the 9 kHz location. Examination of individual two-tone response spectra obtained with f_2 fixed at 9 kHz revealed a complex relationship between the number and amplitude of DP components appearing in the ear canal versus those in the cochlear vibrations (Fig. 5). In general, many more DPs were present in the intracochlear responses than in the ear canal, and DPs at frequencies above f_2 were conspicuously absent from ear-canal spectra. OHC region vibrations exhibited the largest distortions and most broadband distribution of DPs, which were measurable at very low and high frequencies. This confirms recent similar measurements of DPs in gerbil [48, 51] and supports the notion that OHCs are the source of the vibratory DPs. Postmortem measurements verified the physiological origin of the intracochlear DPs and DPOAEs, which were both greatly reduced in magnitude after death and typically not measurable above the noise floor for stimulus levels lower than 70 dB SPL.

While the relative magnitudes of different DP components varied with level, ratio, and measurement location, $2f_1 - f_2$ was typically largest in the ear canal but was often not the dominant intracochlear DP component. The dependence of the intracochlear DP magnitudes on measurement location suggests that various but as yet unidentified mechanisms must influence how DPs are transmitted within the organ of Corti. Furthermore, the dissimilarity between ear-canal and intracochlear DP spectra indicates that DPOAEs are strongly filtered by mechanisms which do not shape DPs near where they are generated.

As a clear demonstration that DPOAEs undergo filtering not experienced by DPs at their generation site, intracochlear DPs showed no evidence of a bandpass shape as the f_2/f_1 ratio was varied. Intracochlear and ear-canal responses from a representative mouse are shown in Fig. 6, with average data ($n = 8$) shown in Fig. 7. For all intracochlear measurement locations, the $2f_1 - f_2$ DP increased as f_1 approached f_2 and was largest at the lowest f_2/f_1 ratios, where DPOAE amplitudes became vanishingly small. The increase in intracochlear DP magnitudes at small f_2/f_1 ratios is consistent with greater nonlinear interactions between the vibrations elicited at the stimulus frequencies, which become more similar in magnitude as f_1 approaches f_2.

DPs measured from the OHC region increased nearly monotonically with decreasing f_2/f_1 ratio, while notches in BM and TM responses were sometimes present at ratios of ~ 1.25–1.3, particularly at lower stimulus levels. Such

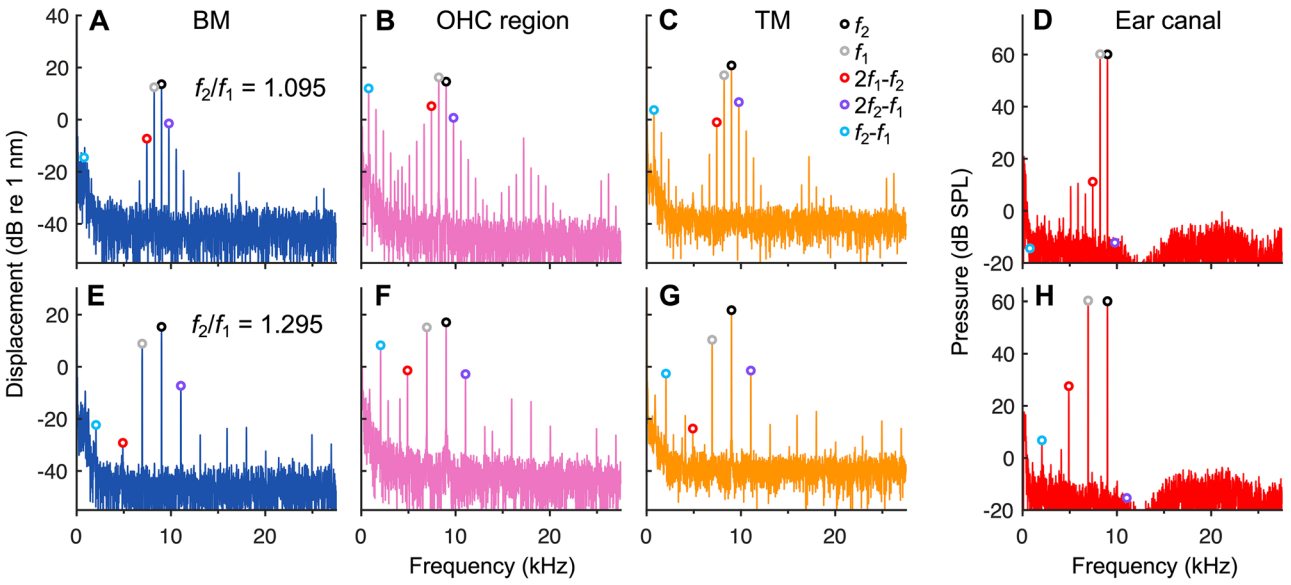

Fig. 5 DPs are strongly filtered as they are transmitted within the organ of Corti and to the ear canal. **A–C** Displacement spectra for the BM, OHC region, and TM in response to two 60 dB SPL stimulus tones, with $f_2 = 9$ kHz and $f_1 = 8.22$ kHz ($f_2/f_1 = 1.095$) for an individual mouse. Peaks corresponding to responses at f_1, f_2, and several DP frequencies are indicated with circles (legend in **C**). In (**A**), the $f_2 - f_1$ component is within the noise floor. **D** Ear-canal pressure spectrum from the same mouse. The number and relative magnitudes of DPs measured in the ear canal are very different from those observed in the vibrations. For example, the $f_2 - f_1$ and $2f_2 - f_1$ DPOAEs are within the noise floor despite these components being present in most of the intracochlear recordings. The dip in the microphone spectrum near 12 kHz is the result of correcting for the frequency response of the probe microphone. **E–H** Same as (**A**)–(**D**), but with $f_1 = 6.95$ kHz ($f_2/f_1 = 1.295$). The $2f_1 - f_2$ DP is the largest component in the ear canal but does not dominate the intracochlear DP spectra

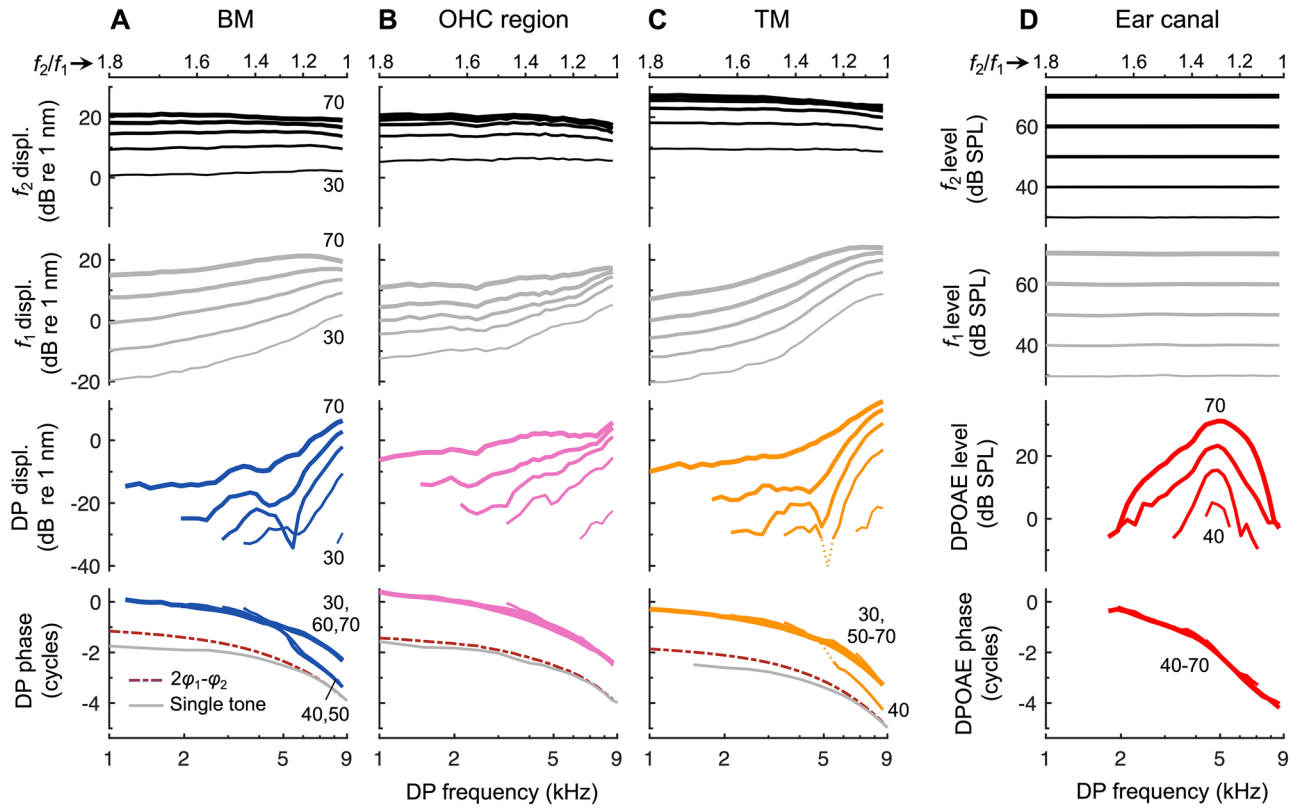

Fig. 6 Intracochlear DPs do not exhibit signs of local bandpass filtering. **A–C** Displacements of the BM, OHC region, and TM in response to two tones, with f_2 fixed at 9 kHz and f_1 varied, and stimuli presented at the same level (30–70 dB SPL in 10 dB steps; indicated by increasing line thickness and numerically for BM responses). Shown are displacement magnitudes at f_2 (top row), f_1 (second row), and $2f_1 - f_2$ (third row), as well as the phase of the $2f_1 - f_2$ DP (bottom row). All responses are plotted vs. the DP frequency with the f_2/f_1 ratio axis provided at the top of each column. For comparison are the phases of single-tone responses over the same frequency range, as well as the expected phases of a locally generated DP (i.e., $2\varphi_1 - \varphi_2$, with φ_1 and φ_2 being the phases of the f_1 and f_2 displacement responses). In (**C**), the dotted portion of the DP response at 40 dB SPL indicates data not meeting the signal-to-noise criterion. **D** As in (**A**)–(**C**) but showing the ear-canal pressure measured in the same mouse. DPOAEs were only measurable at stimulus levels of 40 dB SPL and higher

notches were associated with rapid phase transitions (Fig. 6A, C; bottom row) and may be due to interference between locally generated DPs and DPs that were generated elsewhere and then propagated apically or basally to the measurement site. Indeed, notches occurred near ratios where DPOAEs were largest, suggesting that they may be attributed to the increased strength of a reverse propagating component. Similar notches have been observed in DP ratio functions measured in BM vibrations from gerbil and chinchilla [46, 52].

For OHC region DPs, the lack of prominent notches indicates that these responses were more strongly dominated by a single component – presumably the locally generated DP. DP phases were consistent with the output of a local nonlinearity (dashed-dotted lines in Fig. 6A–C), for which the DP phase takes the form $2\varphi_1 - \varphi_2 + c$, where φ_1 and φ_2 are the phases of inputs at f_1 and f_2, respectively (here taken to be the response phases at f_1 and f_2), and c is either 0 or 180 degrees. However, DP phases also grossly resembled the phases of responses evoked by single tones (solid gray lines in Fig. 6A–C), which would be consistent with the responses being dominated by waves traveling through the measurement site at the DP frequency. Thus, it is difficult to disentangle local vs. propagating DP components based on the phase alone.

Tuning of DPOAE Ratio Functions Is Not Primarily Due to Intracochlear Suppression

In addition to demonstrating the absence of any mechanical resonance that could account for the tuning of DPOAE ratio functions, the intracochlear measurements suggest that the bandpass shape does not arise primarily from nonlinear suppression. When the stimulus tones were presented at the same level, DPOAE amplitudes declined at small f_2/f_1 ratios despite there being little suppression of the f_2 response as f_1 became closer in frequency, and, as noted above, DPs only increased at the smallest f_2/f_1 ratios.

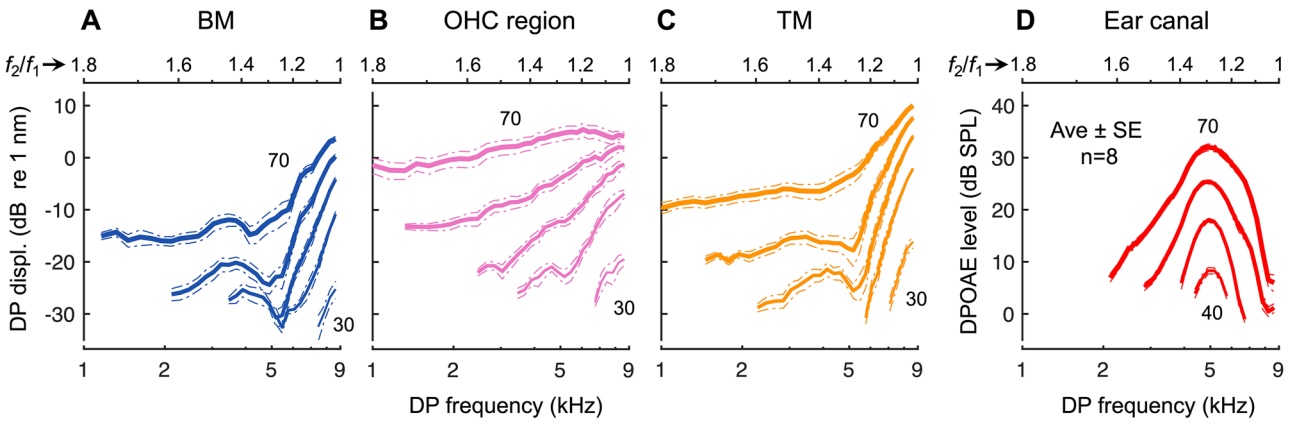

Fig. 7 Average intracochlear DP and ear-canal DPOAE ratio functions. **A**–**D** Average $2f_1 - f_2$ DP amplitudes measured from the BM (**A**), OHC region (**B**), and TM (**C**), and average DPOAEs (**D**) in eight mice. As in Fig. 6, f_2 was fixed at 9 kHz while f_1 was varied, and stimuli were presented at the same level (30–70 dB SPL in 10 dB steps; indicated by increasing line thickness and numerically for the lowest and highest SPLs). Averages only included responses meeting the signal-to-noise criterion and are shown when such data were available in at least four mice. Dashed-dotted lines indicate ± 1 SE. Average DP phases are not shown, as the stimulus levels for which phase shifts occurred were not the same for all mice. However, the general phase patterns were similar across measurements

Nevertheless, to further explore the potential influence of suppression, we also measured intracochlear DP and DPOAE ratio functions with the level of the f_2 tone fixed at 60 dB SPL and the level of the f_1 tone varied from 45 to 75 dB SPL. Figure 8 shows data obtained with this paradigm from the mouse whose individual responses to equal-level stimuli were plotted in Fig. 6, with average data ($n = 9$) shown in Fig. 9. Presenting the f_1 tone at 60 dB SPL or higher could suppress the f_2 response, with suppression being most prominent when f_1 was close in frequency to f_2. However, even for the highest f_1 stimulus level, DPs measured on the BM still tended to increase at small f_2/f_1 ratios, and TM DPs decreased only slightly under these stimulus conditions. While OHC region DP amplitudes were more clearly reduced with decreasing f_2/f_1 ratio when the level of the f_1 tone was at least 10 dB higher than that of f_2, they started to decline at ratios larger than 1.3 and declined more slowly than DPOAE amplitudes as the f_2/f_1 ratio was decreased. Intracochlear suppression therefore does not appear to play a dominant role in the tuning of the DPOAE ratio functions, which retained their sharp, bandpass characteristic regardless of the amount of suppression observed.

This is not to say that DPOAE ratio functions were uninfluenced by suppression, however. For f_2/f_1 ratios smaller than 1.5, DPOAE amplitudes saturated and decreased as the level of the f_1 tone was raised above ~ 70 dB SPL, likely reflecting the saturation and decline observed in the intracochlear DP magnitudes. DPOAEs obtained with the f_1 tone presented at higher levels therefore tended to decline in amplitude more rapidly as f_1 approached f_2. Since the slope of the ratio functions at large f_2/f_1 ratios simultaneously became less steep, Q_{10dB} values underwent small and sometimes nonmonotonic changes as the f_1 stimulus level was increased above 60 dB SPL.

While DPOAE phases were generally similar when obtained with equal- or unequal-level stimuli, presenting the f_2 tone at 60 dB SPL while increasing the level of the f_1 tone produced consistent and large phase leads at small f_2/f_1 ratios. Total phase shifts observed between levels of 60 and 75 dB SPL were maximal near an f_2/f_1 ratio of ~ 1.15 and could approach 1 cycle. These shifts did not appear closely related to changes in the phases of the intracochlear DPs. Complex, level-dependent phase shifts were observed in DPs measured from the BM and TM at ratios where amplitude notches occurred (near an f_2/f_1 of ~ 1.3), while OHC region DPs exhibited consistent, small phase lags (< 0.15 cycles) as the level of the f_1 stimulus exceeded 65 dB SPL. These lags presumably resulted from small phase leads observed in the response at f_2, since the DP phase is expected to follow $2\varphi_1 - \varphi_2$. Similar phase leads have been previously observed in studies of intracochlear suppression [53–55].

Wave Interference Produces Bandpass DPOAE Ratio Functions

The weak correspondence between intracochlear and ear-canal DPs indicates that the tuning of DPOAE ratio functions is not primarily due to local filtering or suppression of DPs near where they are generated. To demonstrate that this filtering occurs instead through a more global, wave interference phenomenon, we used a simple model to estimate the DPOAEs that would be generated as the f_2/f_1 ratio is varied. First, we approximated the BM's spatial response to a given pair of f_1 and f_2 tones, with f_2 fixed at 9 kHz, using BM frequency responses from the 9 kHz region (Fig. 10; see Methods). To generate DPs at each cochlear location, the magnitudes and phases of displacements elicited by the f_1 and f_2 tones were used as those of sinusoidal inputs to a Boltzmann function

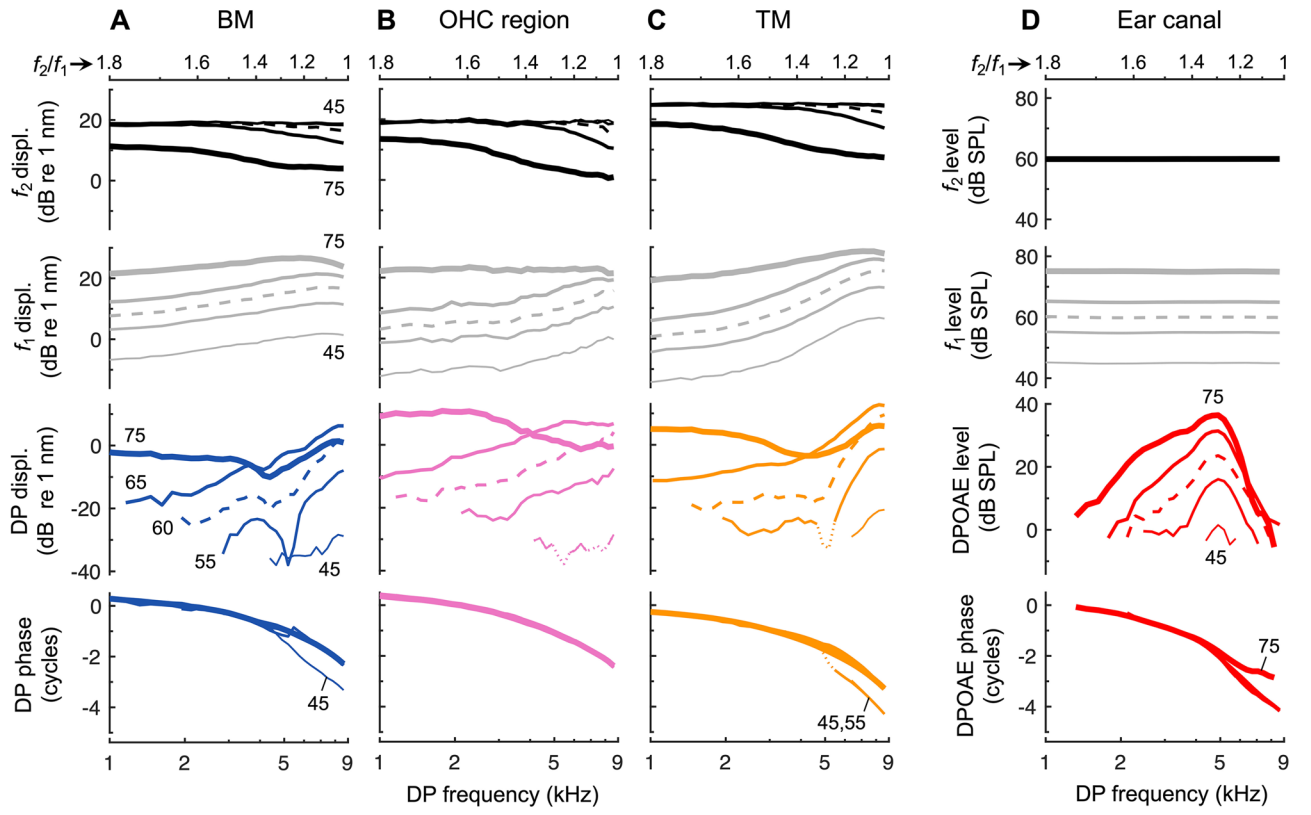

Fig. 8 DPOAE ratio functions are not primarily tuned by intracochlear suppression. **A**–**C** Displacements of the BM, OHC region, and TM in response to two tones with the f_2 tone fixed at 9 kHz and presented at 60 dB SPL, and the f_1 tone varied in both frequency and level (45–75 dB SPL in 5 dB steps; data for f_1 levels of 50 and 70 dB SPL not plotted, for clarity). Shown are displacement magnitudes at f_2 (top row), f_1 (second row), and $2f_1 - f_2$ (third row), as well as the phase of the $2f_1 - f_2$ DP (bottom row) for f_1 tone levels indicated by increasing line thickness and numerically for BM responses. As the level of the f_1 tone increased, the f_2 response was suppressed and DPs could be slightly reduced in magnitude, particularly as f_2/f_1 approached 1. Data are from the same mouse whose responses to equal-level stimuli are shown in Fig. 6. Responses obtained using equal-level stimuli are shown with dashed lines to facilitate comparison. In (**B**) and (**C**), dotted portions of the DP responses indicate data not meeting the signal-to-noise criterion. **D** As in (**A**)–(**C**) but showing the ear-canal pressure. Regardless of the level of the f_1 tone, the decline in DPOAE amplitude at small f_2/f_1 ratios did not resemble that observed for the intracochlear DPs

(Eq. (1)), which approximated the nonlinear relationship between OHC stereociliary displacement and transduction current. Since OHC motility is driven by the transmembrane potential, which is subject to electrical filtering by the OHC membrane, we then low-pass filtered the function's output before determining the magnitude and phase of the resulting $2f_1 - f_2$ DP at each location ($DP_{generated}$; i.e., the DP in the OHC's electromotile output, before it is transmitted to the surrounding structures). Assuming that DPs propagate to the stapes via a wave on the BM, we estimated the magnitude and phase of the DP reaching the stapes from each location (DP_{stapes}) by weighting each generated DP's magnitude by the local BM displacement response to a low-level tone at the DP frequency, and shifting each DP's phase by the local BM response phase (blue lines in Fig. 10). To approximate the DPOAE in the ear canal, DPs arriving at the stapes from each cochlear location were vectorially summed.

At small f_2/f_1 ratios, the estimated spatial responses reveal that the phases of the generated DPs are predicted to vary rapidly with cochlear location (Fig. 10A; bottom panel). Thus, the resulting DP waves would tend to cancel and produce a small DPOAE. The spatial phase variation of the DPs is rapid because the phases of the waves at f_1 and f_2 (i.e., φ_1 and φ_2) vary rapidly in the region where DP generation is maximal. The locally generated DP phase inherits these phases in the form of roughly $2\varphi_1 - \varphi_2$, as mentioned previously. The phase variation is even more rapid after accounting for the reverse travel of each DP to the stapes via a wave at the DP frequency, since the DP frequency is close to f_1. In contrast, for f_2/f_1 ratios near the optimum experimentally observed ratio (Fig. 10B), DP phases are predicted to rotate more slowly over the region where DP generation is strongest. Even though the magnitudes of both the locally generated DPs and the DPs at the stapes are reduced compared to the small f_2/f_1 ratio condition,

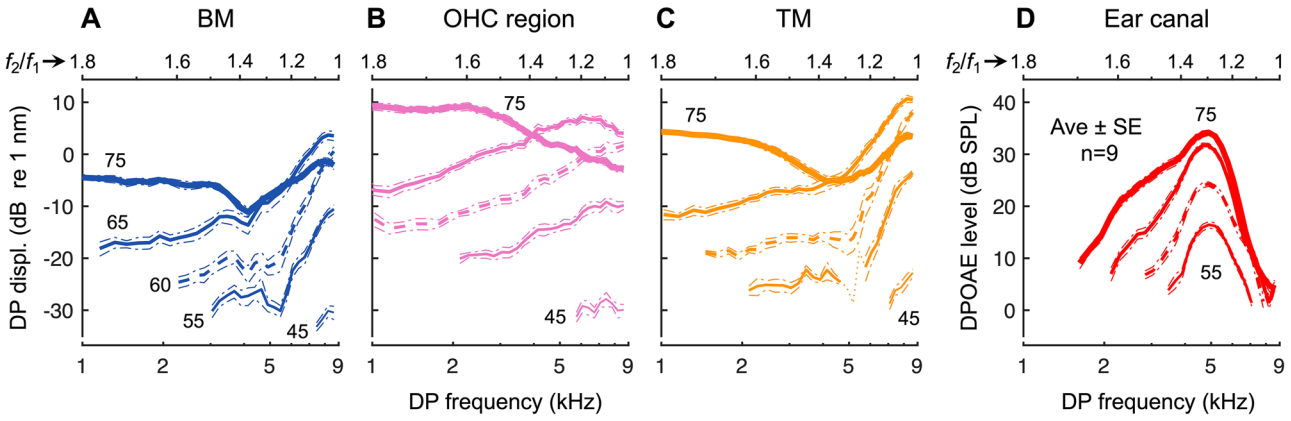

Fig. 9 Average intracochlear DP and ear-canal DPOAE ratio functions obtained with unequal vs. equal stimulus levels. **A**–**C** Average $2f_1 - f_2$ DP amplitudes measured from the BM (**A**), OHC region (**B**), and TM (**C**), and average DPOAEs (**D**) in nine mice for the paradigm in which the f_2 tone was fixed at 9 kHz and presented at 60 dB SPL, while the f_1 tone was varied in both frequency and level (45–75 dB SPL in 5 dB steps; data for 50 and 70 dB SPL not shown, for clarity). The level of the f_1 tone is indicated by increasing line thickness and numerically in (**A**) (curves for the lowest and highest levels are also labeled in **B**–**D**). Dashed lines indicate data obtained with equal-level stimuli. In (**C**), the dotted portion of the curve for the lowest f_1 level indicates where data from fewer than five mice met the signal-to-noise criterion. Dashed-dotted lines indicate ± 1 SE

the DP waves should sum more constructively, thus enhancing the DPOAE amplitude.

At larger f_2/f_1 ratios (Fig. 10C), DPOAEs are predicted to decline in amplitude due to the reduced nonlinear interaction between responses at f_1 and f_2, which generates smaller DPs. DPs arriving at the stapes are expected to be even further attenuated by the BM's low responsiveness to forces generated at the DP frequency (which is ~ 3 kHz when $f_2/f_1 = 1.495$). At least at low stimulus levels, spatial variation in the DP phases is also predicted to be greater than for the optimal f_2/f_1 ratio, which would result in greater destructive interference between the propagating DPs. At high stimulus levels, this phase variation and the degree of interference are diminished, owing to a reduction in the spatial phase gradient of the response at f_2.

By examining the model output across f_2/f_1 ratios, we found that while maximum intracochlear DP magnitudes tended to increase monotonically as f_1 approached f_2, DPOAE amplitudes peaked and started to decline when the spatial phase variation of DPs propagating from the region of maximum generation to the stapes exceeded 0.5 cycles, in agreement with a previous model of human DPOAE generation [24]. Decreasing the f_2/f_1 ratio both increased the rate of DP phase variation and broadened the generation region, due to the greater overlap between the responses to f_1 and f_2. These two effects synergized to facilitate increasingly destructive interference at small f_2/f_1 ratios.

As shown in Fig. 11A, the modeled DPOAE ratio functions exhibited a bandpass shape that was highly similar to that observed in the data, though the functions were slightly broader and peaked at smaller f_2/f_1 ratios. The optimal ratios for the modeled functions were also level dependent, varying from ~ 1.17 to 1.22. Despite these discrepancies, Q_{10dB} values for the modeled DPOAE ratio functions were only ~ 15% lower than those of the average single-tone BM responses used to construct the model, and ~ 21% lower than the measured DPOAE Q_{10dB} values (Fig. 11B). This agreement is perhaps surprising, given that the model does not attempt to mimic the actual physics underlying DPOAE generation, and does not explicitly include the effects of amplification or suppression, or the frequency-dependent influence of middle-ear and ear-canal acoustics. Though such adjustments are arbitrary, we could bring the Q_{10dB} values of the modeled functions within 5–10% of the measured values by simply eliminating the low-pass filtering step, or by weighting the DPs by BM velocity rather than displacement. Increasing the Boltzmann function's slope or operating point parameters by a factor of 2 could also produce up to a ~ 10% increase in Q_{10dB} when averaged across stimulus level. However, these parameter manipulations had little effect on the optimal ratio and general bandpass shape of the modeled functions.

Modeled ratio functions also retained a bandpass shape regardless of whether DPs were assumed to propagate to the stapes via slow waves on the BM or nearly instantaneously through the fluid (i.e., without weighting the DPs by a BM wave at the DP frequency; Fig. 11C). DPOAE ratio functions produced by simply vectorially summing the locally generated DPs exhibited level-dependent changes in tuning sharpness though were much more broadly tuned, with Q_{10dB} values that were ~ 45% lower than the measured values. The propagation route of the DPs may therefore impact the tuning of the ratio functions but is not critical to producing their overall bandpass shape. Instead, the bandpass shape appears to primarily result from spatial variation in the phases of the

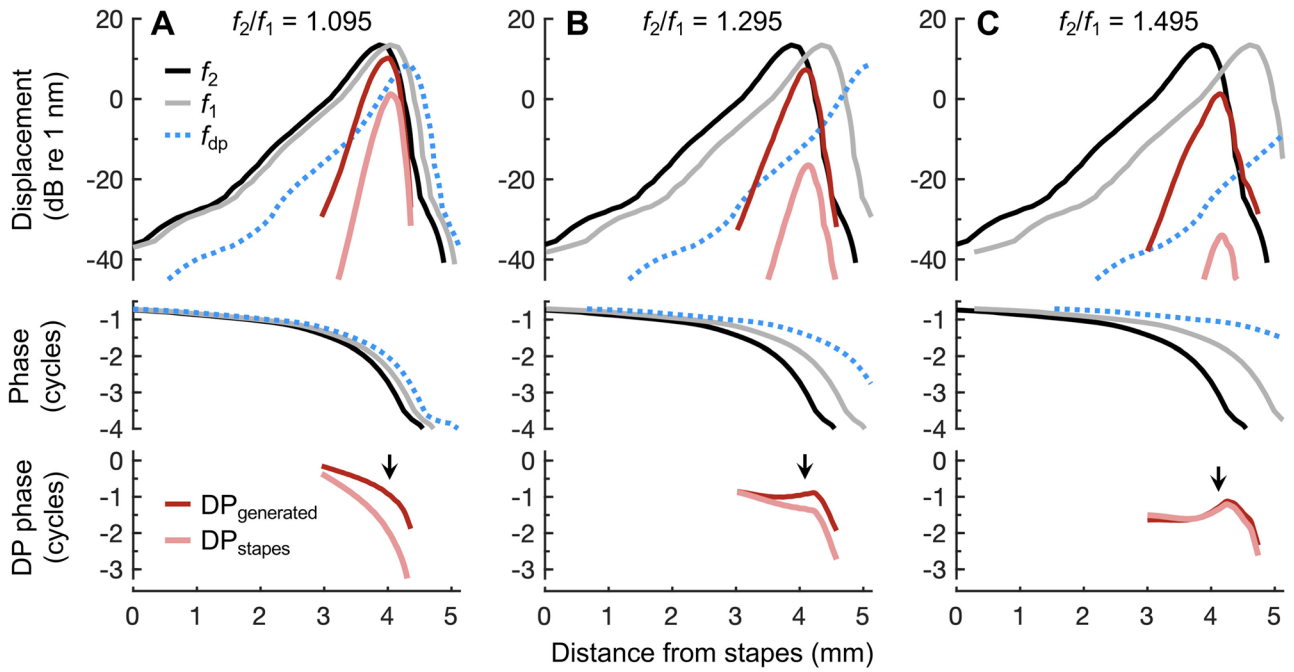

Fig. 10 Spatial variation in DP phase predicts destructive interference at small f_2/f_1 ratios. **A**–**C** Estimated BM displacement magnitudes and phases at f_1 and f_2 as a function of cochlear location for f_2/f_1 ratios of 1.095 (**A**), 1.295 (**B**) and 1.495 (**C**), with stimuli presented at 50 dB SPL. At each location, displacements at f_1 and f_2 were used as the inputs to a Boltzmann function, and the response at $2f_1 - f_2$ in the low-pass filtered output of the function was taken as locally generated DP ($DP_{generated}$; dark red lines). The DP arriving at the stapes from each location (DP_{stapes}; pink lines) was estimated after assuming reverse travel via a wave at the DP frequency (f_{dp}; dotted blue lines). At small ratios, both the local and propagated DPs have phases that vary rapidly as a function of the generation location, resulting in strong wave interference. At ratios closer to or higher than the experimentally observed optimal ratio, the phases vary more slowly with generation location (arrows indicate phase behavior near the location of maximum DP generation). DP magnitudes are arbitrarily scaled, as the output of the Boltzmann function was normalized to 1. Only DP responses with magnitudes within 40 dB of the maximum DP magnitude are shown. Due to the lower DP frequency in (**B**) and (**C**), the wave at f_{dp} peaks abruptly and unrealistically at the apical end of the cochlea. However, this portion of wave falls outside of the DP generation region and is irrelevant to the model's output

stimulus-driven waves, which determines the variation in the phases of the generated DPs and, thus, the degree of interference. As expected, setting all DP phases to 0 prior to vector summation resulted in DPOAE amplitudes that increased with decreasing f_2/f_1 ratio, eliminating the bandpass shape (Fig. 11D). Comparison with ratio functions obtained when DP phases were allowed to vary confirmed that destructive interference not only occurs at small f_2/f_1 ratios, but can also be significant at large ratios. Our simple model therefore illustrates that wave interference strongly influences DPOAE amplitudes and is sufficient to account for the bandpass shape in DPOAE ratio functions.

To verify that the above results extended to other cochlear locations, we also used average vibratory responses from the middle turn to estimate spatial responses and DPOAE ratio functions for an f_2 frequency of 20 kHz. When we included low-pass filtering and BM-weighting of the generated DPs, the modeled DPOAE ratio functions for an f_2 of 20 kHz had an optimum f_2/f_1 ratio of 1.1, only slightly smaller than that observed experimentally. Q_{10dB} values were 15% lower than those of vibratory responses used in the model and 24% lower than the measured DPOAE Q_{10dB}, when averaged across stimulus levels of 50–70 dB SPL. The model therefore replicated the decrease in optimal ratio and increase in Q_{10dB} at higher f_2 frequencies, with the discrepancy between modeled and measured Q_{10dB} values being similar across frequency.

Discussion

Our measurements demonstrate a striking quantitative agreement between the tuning of DPOAE ratio functions and vibratory responses of the BM and TM to single tones in mice. This agreement was maintained across stimulus level and was observed for two cochlear locations with CFs separated by roughly one octave, when ratio functions were obtained with f_2 fixed at the CF. While variability in the morphology of the ratio functions likely precluded their ability to predict small differences in vibratory tuning among normal-hearing mice, the average DPOAE and vibratory tuning values were found to be highly similar. Thus, at least at the population level, DPOAE ratio functions hold promise as a noninvasive window onto cochlear tuning.

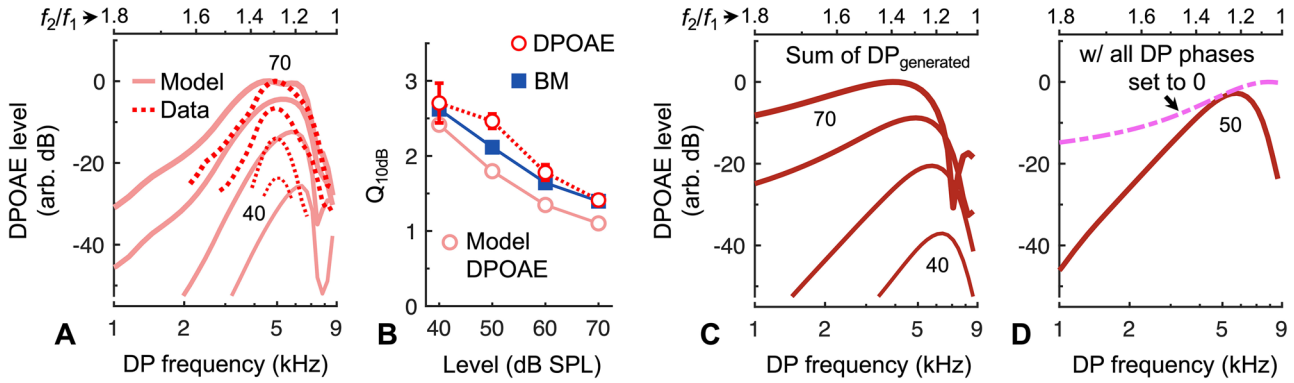

Fig. 11 Bandpass tuning of DPOAE ratio functions is caused by wave interference. **A** Modeled DPOAE ratio functions for 40–70 dB SPL stimuli (10 dB steps) exhibit the bandpass tuning observed in the data. Stimulus level is indicated by line thickness and numerically for the lowest and highest levels. For each f_2/f_1 ratio, DPOAEs were estimated by vectorially summing DPs from all locations after assuming reverse propagation to the stapes via a wave on the BM. DPOAE data are averages from Fig. 7D. **B** Q_{10dB} values of the modeled DPOAE ratio functions increase with decreasing stimulus level and are similar to, but slightly lower than, Q_{10dB} values of the measured DPOAEs (average ± 95% CI from Fig. 3C) and of the average BM displacements used to estimate the spatial responses in the model. **C** Modeled ratio functions still exhibit a bandpass shape when DPOAEs are simply estimated by taking the vector sum of the locally generated DPs (i.e., approximating nearly instantaneous propagation of DPs through the cochlear fluid). The bandpass shape is therefore primarily due to spatial variation in the locally generated DP phase. **D** Comparison of the modeled DPOAE ratio function for 50 dB SPL stimuli from (**C**) with the ratio function obtained when DP phases were all set to 0 prior to vector summation. Without phase variation in the DPs, the resulting DPOAE amplitudes continue to increase with decreasing f_2/f_1 ratio, confirming that bandpass ratio functions arise from wave interference

Measurements of intracochlear DPs provide compelling evidence that DPOAE ratio functions in mice are not primarily tuned by mechanisms that locally shape DPs where they are generated — e.g., suppression [16], TM resonance [13], or the form of the DP-generating nonlinearity [17]. This conclusion is supported by findings in other species, for which near-monotonic growth in DP amplitude as f_1 approaches f_2 has been observed in BM vibrations [46, 52], fluid pressure near the BM [56], and, more recently, in vibrations of the reticular lamina [51]. While DPs measured from the TM in the chinchilla apex have also been reported to grow with decreasing f_2/f_1 ratio [57], these measurements were made from a location tuned to the DP frequency, to which DPs had propagated from their more basal generation sites. Here, we show more directly that the TM does not appear to filter the DPs near where they are generated. While we cannot rule out the potential roles of various tuned micromechanical elements or tuning in vibrational modes that are not captured with our approach, the relevance of these features to the generation and propagation of DPs remains uncertain. We also acknowledge that suppression can indeed influence DPOAE ratio functions, through reductions in the magnitudes of the traveling waves at the stimulus and DP frequencies, as well as small phase changes that may alter how the DP waves interfere. However, such effects do not appear critical for producing bandpass ratio functions.

By estimating the spatial profiles of DP sources and the resulting DPOAE amplitudes, we confirmed that the bandpass shape is instead mainly due to a balance between the influence of two factors: (1) the degree of nonlinear interaction between the stimulus-driven waves, which results in the generation of larger DPs with decreasing f_2/f_1 ratio, and (2) wave interference between DPs generated at different locations. More constructive interference between backward-propagating DP waves occurs near the experimentally observed optimal f_2/f_1 ratio, while destructive interference becomes pronounced at smaller f_2/f_1 ratios, if not also at large f_2/f_1 ratios. Similar conclusions regarding the role of wave interference in shaping DPOAEs have been reached previously through numerous modeling efforts [18–21, 24, 58] and experimental studies [59–61]. However, a link between the tuning of DPOAE ratio functions and cochlear vibrations has only recently been explored in a model of human DPOAE generation [24]. This model predicted that the tuning of DPOAE ratio functions should be correlated with, if not quantitatively similar to BM tuning, as confirmed here in mice.

The origin of the precise, quantitative agreement between DPOAE and vibratory tuning requires further examination. As the tuning of the modeled DPOAE ratio functions depended on assumptions and parameters that were independent of the tuning of the model's responses to the stimulus tones, such an agreement does not appear to be guaranteed. However, at least a correlation between vibratory and DPOAE tuning is anticipated based on the following considerations. First, more sharply tuned responses require smaller f_2/f_1 ratios to elicit nonlinear interactions between the stimulus-driven waves that are sufficient for generating DPs. Second, wave interference between DPs depends on the spatial phase gradients of the waves elicited by f_1 and f_2, which are correlated with tuning sharpness [62, 63].

Specifically, the rate at which $2\varphi_1 - \varphi_2$ varies with cochlear distance plays a critical role, with constructive interference occurring between DP waves when this spatial phase gradient is close to 0, and destructive interference occurring when it significantly departs from this value [20, 21, 24, 58]. Spatial phase gradients can be approximated by the BM phase vs. frequency gradients, which, after being expressed in stimulus periods, increase both with decreasing stimulus level and increasing CF, with greater changes for frequencies near the CF than below the CF. As a result, for more sharply tuned responses, smaller f_2/f_1 ratios are required to achieve gradients in $2\varphi_1 - \varphi_2$ that are close to 0, and the transition from constructive to destructive interference occurs more rapidly with changes in ratio. The ratio functions are therefore tuned to higher DPOAE frequencies and reduced in bandwidth, resulting in higher $Q_{10\text{dB}}$.

While DPOAE and vibratory tuning co-varied across both stimulus level and frequency, optimal f_2/f_1 ratios decreased with increasing frequency but varied little with changes in stimulus level. For a given CF and f_2 frequency, changes in the bandwidth of the ratio functions therefore primarily drove the correspondence between DPOAE and vibratory tuning across stimulus levels. In humans, optimal f_2/f_1 ratios do decrease at lower stimulus levels [11], though not as dramatically as in modeled ratio functions [24]. The discrepancy between modeled and measured optimal ratios is therefore not unique to the present study and may reflect the influence of mechanisms not included in the models, such as suppression, multiple intracochlear reflections of DP waves, or filtering by the middle ear.

Though we focused on comparing vibratory tuning with the tuning of DPOAE ratio functions obtained with equal-level stimuli, we note that DPOAEs are commonly measured using unequal stimulus levels (e.g., as in [24]). The f_1 tone is typically presented at a higher level than the f_2 tone so as to increase the degree of nonlinear interaction between responses at f_1 and f_2 and maximize the DPOAE amplitude. However, by increasing the spatial extent and strength of DP generation, as well as any suppressive effects of the f_1 tone, the use of unequal levels may affect how DPs interfere and thus change the tuning of the DPOAE ratio functions. Consistent with this, in our measurements where the level of the f_2 tone was fixed at 60 dB SPL, increasing the level of the f_1 tone had complex effects on DPOAE ratio function morphology (Figs. 8 and 9). More comprehensive exploration of the parameter space would be useful for understanding the origins of such effects and for optimizing the correlation between DPOAE and vibratory tuning.

Comparisons of DPOAE and vibratory tuning in other species are necessary to determine if a quantitative agreement between the two is a fundamental characteristic of the mammalian cochlea's operation. If so, this may serve as an important constraint on future models, possibly clarifying aspects of OAE generation and propagation. Especially interesting would be measurements in animals whose hearing extends to lower frequencies, as apical responses in such species are much more broadly tuned [64–66], and the mechanics involved in DPOAE generation in these regions may be different. In humans and guinea pigs, the tuning sharpness of DPOAE ratio functions decreases twofold as f_2 is lowered from ~ 10 to 1 kHz [23, 67], suggesting that a correlation between DPOAE and cochlear tuning could extend to apical regions. However, such correlations may be obscured by the fact that ratio functions from other species are often more complex than those reported here, containing multiple strong peaks or sharp notches that are indicative of interference [15, 49, 68]. The origin of these features and how to best avoid or remove them requires further attention.

Whether DPOAE ratio functions can be used to infer cochlear tuning in ears with OHC dysfunction, and presumably broader tuning, is also of key interest. While OHC insult typically leads to reduced DPOAE amplitudes, reported effects on DPOAE ratio functions have been less straightforward. Bandpass tuning is generally preserved in ratio functions from rabbits following noise exposure [69] and from gerbils and mice after treatment with furosemide, an ototoxic drug [50, 70]. Ratio functions from mice with OHC dysfunction have been found to either change little [70] or exhibit complex changes related to the amount of hearing loss, with shifts toward larger optimal f_2/f_1 ratios for moderate losses and de-tuned or low-pass functions (when plotted vs. DP frequency) for more severe losses [71]. For mutant mice in which the TM is detached from the OHCs, ratio functions either retain a bandpass shape or become high-pass [72]. Similarly mixed results have been observed in humans with permanent or temporary hearing loss [73–75].

As direct mechanical measures were not performed in any of the aforementioned studies, conclusions regarding the utility of ratio functions for assessing mechanical tuning in impaired ears are tentative. Still, it is conceivable that diverse patterns of OHC damage produce similarly diverse effects on how DP waves interfere, leading to complex effects on ratio function morphology. Additionally, certain mutations affecting the TM and OHC stereocilia have actually been found to increase the active or passive tuning of cochlear vibrations [76, 77]. Further measurement and modeling of responses in impaired ears are therefore necessary to assess how ratio functions from such ears specifically relate to mechanical tuning. Such work should carefully consider how the spatial extent of DP generation and the DP propagation route may be affected in ears with OHC dysfunction, particularly at the higher stimulus levels that are required to elicit responses in these ears.

At least in normal-hearing mice, our comparisons of intracochlear and ear canal DPs (Fig. 5) support the view that DPs propagate to the stapes via slow, BM-coupled traveling waves. Primary evidence for this was that DP components at frequencies significantly above f_2 (with $f_2 = \mathrm{CF}$) were abundant inside of the cochlea but nearly absent in the ear canal. This is presumably because the BM within the DP generation region cannot support slow, traveling waves at frequencies much higher than the CF. If DPs instead propagated mainly through fast waves in the fluid, one might expect to measure more of the high-frequency components in the ear canal. Assuming that DPs in the motions of the OHC region (or TM) are not directly coupled to the stapes through the fluid, then the transmission of lower-frequency DPs to the ear canal is likely also shaped by BM mechanics. Thus, even if OHCs in basal regions produce $2f_1 - f_2$ DPs in response to low-frequency stimuli, the contribution of these components to the total reverse-propagating DP wave will be attenuated by the underlying BM's weak response to forces at the DP frequency, which will fall far below the local CF. The BM and its fluid interactions are therefore expected to restrict the basal extent of DPs contributing significantly to the DPOAE, as suggested by recent modeling work [38, 78]. Whether alternative modes of DP propagation and/or contributions from basal OHC sources become more influential under certain stimulus conditions or in pathological ears remains to be determined.

Acknowledgements This work was supported by a Hearing Health Foundation Emerging Research grant (J.B.D.) and NIH/NIDCD grants R21 DC019209 (J.B.D.) and R01 DC003687 (C.A.S.). We thank Drs. John Oghalai and Brian Applegate for providing the OCT system used to collect the data, Alessandro Altoè for helpful discussions, and three anonymous reviewers who provided valuable feedback on the manuscript.

Funding Open access funding provided by SCELC, Statewide California Electronic Library Consortium

Data Availability All data used to support the conclusions in this manuscript are available at https://github.com/jbdewey/Dewey2023JARO.

Declarations

Competing Interests The authors declare no competing interests.

Open Access This article is licensed under a Creative Commons Attribution 4.0 International License, which permits use, sharing, adaptation, distribution and reproduction in any medium or format, as long as you give appropriate credit to the original author(s) and the source, provide a link to the Creative Commons licence, and indicate if changes were made. The images or other third party material in this article are included in the article's Creative Commons licence, unless indicated otherwise in a credit line to the material. If material is not included in the article's Creative Commons licence and your intended use is not permitted by statutory regulation or exceeds the permitted use, you will need to obtain permission directly from the copyright holder. To view a copy of this licence, visit http://creativecommons.org/licenses/by/4.0/.

References

1. Robles L, Ruggero MA (2001) Mechanics of the mammalian cochlea. Physiol Rev 81:1305–1352. https://doi.org/10.1152/physrev.2001.81.3.1305
2. von Békésy G (1960) Experiments in Hearing. McGraw-Hill, USA, New York
3. Ashmore J (2008) Cochlear outer hair cell motility. Physiol Rev 88:173–210. https://doi.org/10.1152/physrev.00044.2006
4. Brownell WE, Bader CR, Bertrand D, de Ribaupierre Y (1985) Evoked mechanical responses of isolated cochlear outer hair cells. Science 227:194–196. https://doi.org/10.1126/science.3966153
5. Dewey JB, Applegate BE, Oghalai JS (2019) Amplification and suppression of traveling waves along the mouse organ of Corti: evidence for spatial variation in the longitudinal coupling of outer hair cell-generated forces. J Neurosci 39:1805–1816. https://doi.org/10.1523/JNEUROSCI.2608-18.2019
6. Rhode WS (1971) Observations of the vibration of the basilar membrane in squirrel monkeys using the Mössbauer technique. J Acoust Soc Am 49:1218–1231. https://doi.org/10.1121/1.1912485
7. Avan P, Büki B, Petit C (2013) Auditory distortions: origins and functions. Physiol Rev 93:1563–1619. https://doi.org/10.1152/physrev.00029.2012
8. Kemp DT (1979) Evidence of mechanical nonlinearity and frequency selective wave amplification in the cochlea. Arch Otorhinolaryngol 224:37–45. https://doi.org/10.1007/BF00455222
9. Brown AM, Gaskill SA (1990) Measurement of acoustic distortion reveals underlying similarities between human and rodent mechanical responses. J Acoust Soc Am 88:840–849. https://doi.org/10.1121/1.399733
10. Fahey P, Allen J (1986) Characterization of cubic intermodulation distortion products in the cat external auditory meatus. In: Allen J, Hall J, Hubbard A et al (eds) Peripheral Auditory Mechanisms. Springer-Verlag, Berlin, pp 314–321
11. Harris FP, Lonsbury-Martin BL, Stagner BB et al (1989) Acoustic distortion products in humans: systematic changes in amplitudes as a function of f_2/f_1 ratio. J Acoust Soc Am 85:220–229. https://doi.org/10.1121/1.397728
12. Kim DO (1980) Cochlear mechanics: implications of electrophysiological and acoustical observations. Hear Res 2:297–317. https://doi.org/10.1016/0378-5955(80)90064-7
13. Allen JB, Fahey PF (1993) A second cochlear-frequency map that correlates distortion product and neural tuning measurements. J Acoust Soc Am 94:809–816. https://doi.org/10.1121/1.408182
14. Brown A, Williams D (1993) A second filter in the cochlea. In: Duifhuis J, van Dijk P, van Netten SM (eds) Biophysics of Hair Cell Sensory Systems. World Scientific, Singapore, pp 72–77
15. Lukashkin AN, Smith JK, Russell IJ (2007) Properties of distortion product otoacoustic emissions and neural suppression tuning curves attributable to the tectorial membrane resonance. J Acoust Soc Am 121:337–343. https://doi.org/10.1121/1.2390670
16. Kanis LJ, de Boer E (1997) Frequency dependence of acoustic distortion products in a locally active model of the cochlea. J Acoust Soc Am 101:1527–1531. https://doi.org/10.1121/1.418173
17. Lukashkin AN, Russell IJ (2001) Origin of the bell-like dependence of the DPOAE amplitude on primary frequency ratio. J Acoust Soc Am 110:3097–3106. https://doi.org/10.1121/1.1417525
18. Matthews JW, Molnar CE (1986) Modeling intracochlear and ear canal distortion product ($2f_1$–f_2). In: Allen JB, Hall JL, Hubbard AE et al (eds) Peripheral Auditory Mechanisms. Springer, Berlin, pp 258–265
19. Neely ST, Stover LJ (1997) Generation of distortion products in a model of cochlear mechanics. In: Lewis E, Long G, Lyon R et al (eds) Diversity in Auditory Mechanics. World Scientific, Singapore, pp 434–440

20. Shera CA (2003) Wave interference in the generation of reflection- and distortion-source emissions. In: Gummer AW (ed) Biophysics of the Cochlea: From Molecules to Models. World Scientific, Singapore, pp 439–453
21. Talmadge CL, Tubis A, Long GR, Piskorski P (1998) Modeling otoacoustic emission and hearing threshold fine structures. J Acoust Soc Am 104:1517–1543. https://doi.org/10.1121/1.424364
22. Brown AM, Gaskill SA, Carlyon RP, Williams DM (1993) Acoustic distortion as a measure of frequency selectivity: relation to psychophysical equivalent rectangular bandwidth. J Acoust Soc Am 93:3291–3297. https://doi.org/10.1121/1.405713
23. Wilson US, Browning-Kamins J, Durante AS et al (2021) Cochlear tuning estimates from level ratio functions of distortion product otoacoustic emissions. Int J Audiol 60:890–899. https://doi.org/10.1080/14992027.2021.1886352
24. Sisto R, Wilson US, Dhar S, Moleti A (2018) Modeling the dependence of the distortion product otoacoustic emission response on primary frequency ratio. J Assoc Res Otolaryngol 19:511–522. https://doi.org/10.1007/s10162-018-0681-9
25. Dewey JB, Altoe A, Shera CA et al (2021) Cochlear outer hair cell electromotility enhances organ of Corti motion on a cycle-by-cycle basis at high frequencies in vivo. Proc Natl Acad Sci USA 118:e2025206118. https://doi.org/10.1073/pnas.2025206118
26. Lee HY, Raphael PD, Park J et al (2015) Noninvasive in vivo imaging reveals differences between tectorial membrane and basilar membrane traveling waves in the mouse cochlea. Proc Natl Acad Sci USA 112:3128–3133. https://doi.org/10.1073/pnas.1500038112
27. Lee HY, Raphael PD, Xia A et al (2016) Two-dimensional cochlear micromechanics measured in vivo demonstrate radial tuning within the mouse organ of Corti. J Neurosci 36:8160–8173. https://doi.org/10.1523/JNEUROSCI.1157-16.2016
28. Soons JAMM, Ricci AJ, Steele CR, Puria S (2015) Cytoarchitecture of the mouse organ of corti from base to apex, determined using in situ two-photon imaging. J Assoc Res Otolaryngol 16:47–66. https://doi.org/10.1007/s10162-014-0497-1
29. Taberner AM, Liberman MC (2005) Response properties of single auditory nerve fibers in the mouse. J Neurophysiol 93:557–569. https://doi.org/10.1152/jn.00574.2004
30. Shera CA, Guinan JJ (1999) Evoked otoacoustic emissions arise by two fundamentally different mechanisms: a taxonomy for mammalian OAEs. J Acoust Soc Am 105:782–798. https://doi.org/10.1121/1.426948
31. Cheatham MA (2021) Comparing spontaneous and stimulus frequency otoacoustic emissions in mice with tectorial membrane defects. Hear Res 400:108143. https://doi.org/10.1016/j.heares.2020.108143
32. Martin GK, Stagner BB, Chung YS, Lonsbury-Martin BL (2011) Characterizing distortion-product otoacoustic emission components across four species. J Acoust Soc Am 129:3090–3103. https://doi.org/10.1121/1.3560123
33. Müller M, von Hünerbein K, Hoidis S, Smolders JWT (2005) A physiological place-frequency map of the cochlea in the CBA/J mouse. Hear Res 202:63–73. https://doi.org/10.1016/j.heares.2004.08.011
34. Housley GD, Ashmore JF (1992) Ionic currents of outer hair cells isolated from the guinea-pig cochlea. J Physiol 448:73–98. https://doi.org/10.1113/jphysiol.1992.sp019030
35. Russell IJ, Cody AR, Richardson GP (1986) The responses of inner and outer hair cells in the basal turn of the guinea-pig cochlea and in the mouse cochlea grown in vitro. Hear Res 22:199–216. https://doi.org/10.1016/0378-5955(86)90096-1
36. Santos-Sacchi J (1989) Asymmetry in voltage-dependent movements of isolated outer hair cells from the organ of Corti. J Neurosci 9:2954–2962. https://doi.org/10.1523/jneurosci.09-08-02954.1989
37. Dewey JB (2022) Cubic and quadratic distortion products in vibrations of the mouse cochlear apex. JASA Express Lett 2:11440. https://doi.org/10.1121/10.0015244
38. Bowling T, Wen H, Meenderink SWF, Dong W (2021) Intracochlear distortion products are broadly generated by outer hair cells but their contributions to otoacoustic emissions are spatially restricted. Sci Rep 11:13651. https://doi.org/10.1038/s41598-021-93099-7
39. Bowling T, Meaud J (2018) Forward and reverse waves: Modeling distortion products in the intracochlear fluid pressure. Biophys J 114:747–757. https://doi.org/10.1016/j.bpj.2017.12.005
40. Dong W, Olson ES (2008) Supporting evidence for reverse cochlear traveling waves. J Acoust Soc Am 123:222–240. https://doi.org/10.1121/1.2816566
41. Meenderink SWF, van der Heijden M (2010) Reverse cochlear propagation in the intact cochlea of the gerbil: evidence for slow traveling waves. J Neurophysiol 103:1448–1455. https://doi.org/10.1152/jn.00899.2009
42. Moleti A, Sisto R (2008) Comparison between otoacoustic and auditory brainstem response latencies supports slow backward propagation of otoacoustic emissions. J Acoust Soc Am 123:1495–1503. https://doi.org/10.1121/1.2836781
43. Shera CA, Tubis A, Talmadge CL et al (2007) Allen-Fahey and related experiments support the predominance of cochlear slow-wave otoacoustic emissions. J Acoust Soc Am 121:1564–1575. https://doi.org/10.1121/1.2405891
44. Vetesník A, Gummer AW (2012) Transmission of cochlear distortion products as slow waves: a comparison of experimental and model data. J Acoust Soc Am 131:3914–3934. https://doi.org/10.1121/1.3699207
45. He W, Fridberger A, Porsov E, Ren T (2010) Fast reverse propagation of sound in the living cochlea. Biophys J 98:2497–2505. https://doi.org/10.1016/j.bpj.2010.03.003
46. Ren T (2004) Reverse propagation of sound in the gerbil cochlea. Nat Neurosci 7:333–334. https://doi.org/10.1038/nn1216
47. Shera CA, Talmadge CL, Tubis A (2000) Interrelations among distortion-product phase-gradient delays: their connection to scaling symmetry and its breaking. J Acoust Soc Am 108:2933–2948. https://doi.org/10.1121/1.1323234
48. Vavakou A, Cooper NP, van der Heijden M (2019) The frequency limit of outer hair cell motility measured in vivo. Elife 8:e47667. https://doi.org/10.7554/eLife.47667
49. Burwood GWS, Russell IJ, Lukashkin AN (2017) Rippling pattern of distortion product otoacoustic emissions evoked by high-frequency primaries in guinea pigs. J Acoust Soc Am 142:855–862. https://doi.org/10.1121/1.4998584
50. Mills DM, Rubel EW (1997) Development of distortion product emissions in the gerbil: "Filter" response and signal delay. J Acoust Soc Am 101:395–411. https://doi.org/10.1121/1.417985
51. Ren T, He W (2020) Two-tone distortion in reticular lamina vibration of the living cochlea. Commun Biol 3:35. https://doi.org/10.1038/s42003-020-0762-2
52. Rhode WS (2007) Distortion product otoacoustic emissions and basilar membrane vibration in the 6–9 kHz region of sensitive chinchilla cochleae. J Acoust Soc Am 122:2725–2737. https://doi.org/10.1121/1.2785034
53. Cooper NP (1996) Two-tone suppression in cochlear mechanics. J Acoust Soc Am 99:3087–3098. https://doi.org/10.1121/1.414795
54. Nuttall AL, Dolan DF (1993) Two-tone suppression of inner hair cell and basilar membrane responses in the guinea pig. J Acoust Soc Am 93:390–400. https://doi.org/10.1121/1.405619
55. Rhode WS, Cooper NP (1993) Two-tone suppression and distortion production on the basilar membrane in the hook region of cat and guinea pig cochleae. Hear Res 66:31–45. https://doi.org/10.1016/0378-5955(93)90257-2

56. Dong W, Olson ES (2005) Two-tone distortion in intracochlear pressure. J Acoust Soc Am 117:2999–3015. https://doi.org/10.1121/1.1880812
57. Cooper NP, Rhode WS (1997) Mechanical responses to two-tone distortion products in the apical and basal turns of the mammalian cochlea. J Neurophysiol 78:261–270. https://doi.org/10.1152/jn.1997.78.1.261
58. Shera CA, Guinan JJ (2007) Cochlear traveling-wave amplification, suppression, and beamforming probed using noninvasive calibration of intracochlear distortion sources. J Acoust Soc Am 121:1003–1016. https://doi.org/10.1121/1.2404620
59. Fahey PF, Stagner BB, Martin GK (2006) Mechanism for bandpass frequency characteristic in distortion product otoacoustic emission generation. J Acoust Soc Am 119:991–996. https://doi.org/10.1121/1.2146088
60. Martin GK, Stagner BB, Dong W, Lonsbury-Martin BL (2016) Comparing distortion product otoacoustic emissions to intracochlear distortion products inferred from a noninvasive assay. J Assoc Res Otolaryngol 17:271–287. https://doi.org/10.1007/s10162-016-0552-1
61. Martin GK, Stagner BB, Lonsbury-Martin BL (2013) Time-domain demonstration of distributed distortion-product otoacoustic emission components. J Acoust Soc Am 134:342–355. https://doi.org/10.1121/1.4809676
62. Charaziak KK, Shera CA (2021) Reflection-source emissions evoked with clicks and frequency sweeps: comparisons across levels. J Assoc Res Otolaryngol 22:641–658. https://doi.org/10.1007/s10162-021-00813-3
63. Shera CA, Charaziak KK (2019) Cochlear frequency tuning and otoacoustic emissions. Cold Spring Harb Perspect Med 9:a033498. https://doi.org/10.1101/cshperspect.a033498
64. Cooper NP, Rhode WS (1995) Nonlinear mechanics at the apex of the guinea-pig cochlea. Hear Res 82:225–243. https://doi.org/10.1016/0378-5955(94)00180-x
65. Dong W, Xia A, Raphael PD et al (2018) Organ of Corti vibration within the intact gerbil cochlea measured by volumetric optical coherence tomography and vibrometry. J Neurophysiol 120:2847–2857. https://doi.org/10.1152/jn.00702.2017
66. Recio-Spinoso A, Oghalai JS (2017) Mechanical tuning and amplification within the apex of the guinea pig cochlea. J Physiol 595:4549–4561. https://doi.org/10.1113/JP273881
67. Schneider S, Schoonhoven R, Prijs VF (2001) Amplitude of distortion product otoacoustic emissions in the guinea pig in f(1)- and f(2)-sweep paradigms. Hear Res 155:21–31. https://doi.org/10.1016/s0378-5955(01)00239-8
68. Mills DM (2000) Frequency responses of two- and three-tone distortion product otoacoustic emissions in Mongolian gerbils. J Acoust Soc Am 107:2586–2602. https://doi.org/10.1121/1.428646
69. Ohlms LA, Lonsbury-Martin BL, Martin GK (1991) Acoustic-distortion products: separation of sensory from neural dysfunction in sensorineural hearing loss in human beings and rabbits. Otolaryngol Head Neck Surg 104:159–174. https://doi.org/10.1177/019459989110400203
70. Konrad-Martin D, Norton SJ, Mascher KE, Tempel BL (2001) Effects of PMCA2 mutation on DPOAE amplitudes and latencies in deafwaddler mice. Hear Res 151:205–220. https://doi.org/10.1016/S0378-5955(00)00228-8
71. Le Calvez S, Guilhaume A, Romand R et al (1998) CD1 hearing-impaired mice. II: Group latencies and optimal f_2/f_1 ratios of distortion product otoacoustic emissions, and scanning electron microscopy. Hear Res 120:51–61. https://doi.org/10.1016/S0378-5955(98)00051-3
72. Lukashkin AN, Lukashkina VA, Legan PK et al (2004) Role of the tectorial membrane revealed by otoacoustic emissions recorded from wild-type and transgenic $Tecta^{\Delta ENT/\Delta ENT}$ mice. J Neurophysiol 91:163–171. https://doi.org/10.1152/jn.00680.2003
73. Brown AM, Williams DM, Gaskill SA (1993) The effect of aspirin on cochlear mechanical tuning. J Acoust Soc Am 93:3298–3307. https://doi.org/10.1121/1.405714
74. Engdahl B, Kemp DT (1996) The effect of noise exposure on the details of distortion product otoacoustic emissions in humans. J Acoust Soc Am 99:1573–1587. https://doi.org/10.1121/1.414733
75. Stover LJ, Neely ST, Gorga MP (1999) Cochlear generation of intermodulation distortion revealed by DPOAE frequency functions in normal and impaired ears. J Acoust Soc Am 106:2669–2678. https://doi.org/10.1121/1.428097
76. Dewey JB, Xia A, Müller U et al (2018) Mammalian auditory hair cell bundle stiffness affects frequency tuning by increasing coupling along the length of the cochlea. Cell Rep 23:2915–2927. https://doi.org/10.1016/j.celrep.2018.05.024
77. Russell IJ, Legan PK, Lukashkina VA et al (2007) Sharpened cochlear tuning in a mouse with a genetically modified tectorial membrane. Nat Neurosci 10:215–223. https://doi.org/10.1038/nn1828
78. Moleti A, Sisto R (2020) Does the "reticular lamina nonlinearity" contribute to the basal DPOAE source? J Assoc Res Otolaryngol 21:463–473. https://doi.org/10.1007/s10162-020-00771-2

Publisher's Note Springer Nature remains neutral with regard to jurisdictional claims in published maps and institutional affiliations.